Kinetics and dynamics of processes at surfaces

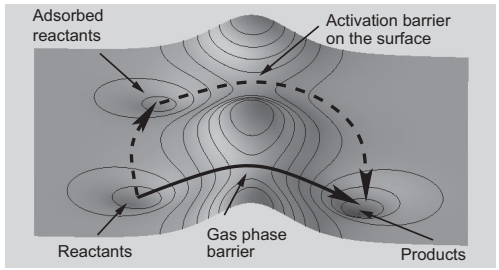

Schematic sketch of the role of a catalyst

Potential energy surface crucial quantity in order to understand the kinetics and dynamics of adsorbates and reactions

Experiment: Potential energy surface (PES) never directly measured but just reaction rates and probabilities

Static information from total-energy calculations often not sufficient to understand how a process proceeds

⇒ Kinetic or dynamical simulation of the reaction
Allows a true comparison with experiment and a reliable check of the accuracy of the calculated PES

In principle, quantum dynamical studies have to be performed to simulate atomic motion, but often classical molecular dynamics studies are sufficient

Classical molecular dynamics

Numerical integration of the equation of motion

Newton

$$M_i \frac{\partial^2}{\partial t^2}\vec{R}_i = -\frac{\partial}{\partial \vec{R}_i} V(\{\vec{R}_j\}). \tag{161}$$

Hamilton

$$\dot{q} = \frac{\partial H}{\partial p} \quad \dot{p} = -\frac{\partial H}{\partial q} \tag{162}$$

Numerical integration schemes:
Runge-Kutta
Burlirsch-Stoer
Predictor-Corrector
Verlet

Verlet Algorithmus

Verlet algorithm easily derived from a Taylor expansion of the trajectory

$$\vec{r}_i(t+h) = 2\vec{r}_i(t) - \vec{r}_i(t-h) + h^2 \frac{\vec{F}_i(t)}{m} + O(h^4) \tag{163}$$

Note that the velocity does not explicitly appear
It can be estimated as

$$\vec{v}_i(t) = \frac{\vec{r}_i(t+h) - \vec{r}_i(t-h)}{2h}. \tag{164}$$

Kinetic energy evaluated with (164) belongs to the time step prior to the one used for the positions (163)

Kinetic and potential energy can be evaluated for the same time step using the velocity Verlet algorithm which is mathematically equivalent to (163)

$$\begin{aligned} \vec{r}_i(t+h) &= \vec{r}_i(t) + h\,\vec{v}_i(t) + \frac{h^2}{2}\frac{\vec{F}_i(t)}{m} \\ \vec{v}_i(t+h) &= \vec{v}_i(t) + h\,\frac{\vec{F}_i(t+h) + \vec{F}_i(t)}{2m} \end{aligned} \tag{165}$$

Time step in molecular dynamics runs

Error associated with time step h in Verlet algorithm:

$$O(h^4)$$

Shorter time steps increase accuracy *per time step*,
but also increase the computational cost

Furthermore, the error of each time step may accumulate.

Accuracy of numerical integration of the equation of motion can be checked by testing the conservation of the total energy

Rule of the thumb:
time step should be ten times smaller than the shortest vibrational or rotational period of a given system

Example: period of H-H vibration $\tau_{vib} \approx 8$ fs
$\Rightarrow h \leq 0.8$ fs

Time-independent quantum dynamics

Time-independent Schrödinger equation

$$(H \; - \; E) \; \Psi \; = \; 0, \tag{166}$$

Choose one specific reaction path coordinate s

$$(\frac{-\hbar^2}{2\mu}\partial_s^2 \; + \; \tilde{H} \; - E) \; \Psi \; = \; 0. \tag{167}$$

Expand the wave function in the coordinates perpendicular to the reaction path coordinate in some suitable set of basis functions

$$\Psi \; = \Psi(s, \ldots) \; = \; \sum_n \; \psi_n(s) \; |n\rangle. \tag{168}$$

Insert the expansion of Ψ in (167) and multiply the Schrödinger equation by $\langle m|$
$\Rightarrow$ Coupled-channel equations

$$\sum_n \left\{ (\frac{-\hbar^2}{2\mu}\partial_s^2 \; - \; E) \; \delta_{m,n} + \; \langle m|\tilde{H}|n\rangle \right\} \; \psi_n(s) \; = \; 0. \tag{169}$$

Instead of a partial differential equation – the original time-independent Schrödinger equation (166) – we now have a set of coupled ordinary differential equation.

Time-dependent quantum dynamics

Time-dependent Schrödinger equation

$$i\hbar \; \frac{\partial}{\partial t} \; \Psi(\vec{R}, t) \; = \; H \; \Psi(\vec{R}, t) \tag{170}$$

For a time-independent Hamiltonian, the solution can be formally written as

$$\Psi(\vec{R}, t) \; = \; e^{-iHt/\hbar} \; \Psi(\vec{R}, t = 0), \tag{171}$$

Two common approaches to represent the time-evolution operator $\exp(-iHt/\hbar)$
i) split-operator method

$$e^{-iH\Delta t/\hbar} \; = \; e^{-iT\Delta t/2\hbar} \; e^{-iV\Delta t/\hbar} \; e^{-iT\Delta t/2\hbar} \; + \; O(\Delta t^3), \tag{172}$$

ii) Chebyshev method

$$e^{-iH\Delta t/\hbar} \; = \; \sum_{j=1}^{j_{\max}} \; a_j(\Delta t) \; T_j(\bar{H}), \tag{173}$$

T_j Chebyshev polynomials, $\bar{H}$ rescaled Hamiltonian

Kinetic energy operator T diagonal in $\vec{k}$-space and potential V in real-space
$\rightarrow$ Fast Fourier Transformations (FFT)

Inelastic scattering of atoms and molecules

Summary of the different collision process in nonreactive scattering:

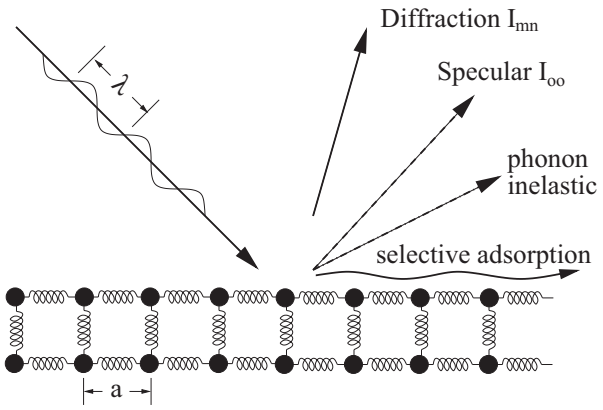

Scattering of light atoms and molecules: Diffraction

Light atoms and molecules scattered at periodic surfaces:
$\Rightarrow$ elastic scattering and diffraction if $\lambda \approx a$

Momentum conservation parallel to the surface:

$$\vec{K}_f^{\parallel} \; = \vec{K}_i^{\parallel} \; + \; \Delta\vec{G}_{mn} \; , \tag{174}$$

with reciprocal lattice vector $\Delta\vec{G}_{mn}$ of the surface

Energy conservation for elastic scattering of atoms:

$$\frac{\hbar^2\vec{K}_f^2}{2M} \; = \; \frac{\hbar^2\vec{K}_i^2}{2M} \tag{175}$$

Final scattering angles entirely determined by the geometry of the surface

Inelastic scattering of atoms and molecules

Excitation and deexcitation of substrate phonons in the scattering events:
$\Rightarrow$ inelastic scattering and diffraction

Momentum conservation parallel to the surface:

$$\vec{K}_f^{\parallel} = \vec{K}_i^{\parallel} + \Delta\vec{G}_{mn} + \sum_{\text{exch.phon.}} \pm\vec{Q}, \qquad (176)$$

$\vec{Q}$ two-dimensional phonon-momentum vector

Energy conservation for inelastic scattering of atoms:

$$\frac{\hbar^2\vec{K}_f^2}{2M} = \frac{\hbar^2\vec{K}_i^2}{2M} + \sum_{\text{exch.phon.}} \pm\hbar\omega_{\vec{Q},j} \qquad (177)$$

Molecular scattering: additional excitation of internal degrees of freedom

$$\frac{\hbar^2\vec{K}_f^2}{2M} = \frac{\hbar^2\vec{K}_i^2}{2M} + \Delta E_{\text{rot}} + \Delta E_{\text{vib}} + \sum_{\text{exch.phon.}} \pm\hbar\omega_{\vec{Q},j} \qquad (178)$$

Rotationally inelastic scattering: H_2/Pd(100)

A. Groß and M. Scheffler, CPL **263**, 567 (1996)

In-plane scattering

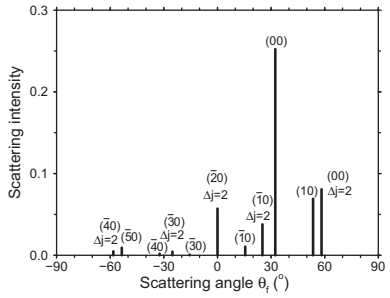

Out of plane scattering

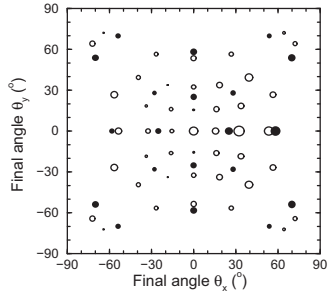

● Rotationally elastic, ○ rotationally inelastic scattering.

Specular peak most pronounced,
but strong off-specular and rotationally inelastic diffraction intensities
$\Rightarrow$ Corrugation and anisotropy of the PES

Inelastic scattering of atoms and molecules

Excitation and deexcitation of substrate phonons in the scattering events:
$\Rightarrow$ inelastic scattering and diffraction

Energy and momentum conservation parallel to the surface
($\vec{Q}$ 2D phonon-momentum vector):

$$\frac{\hbar^2\vec{K}_f^2}{2M} = \frac{\hbar^2\vec{K}_i^2}{2M} + \sum_{\text{exch.phon.}} \pm\hbar\omega_{\vec{Q},j}, \qquad \vec{K}_f^{\parallel} = \vec{K}_i^{\parallel} + \Delta\vec{G}_{mn} + \sum_{\text{exch.phon.}} \pm\vec{Q}, \qquad (179)$$

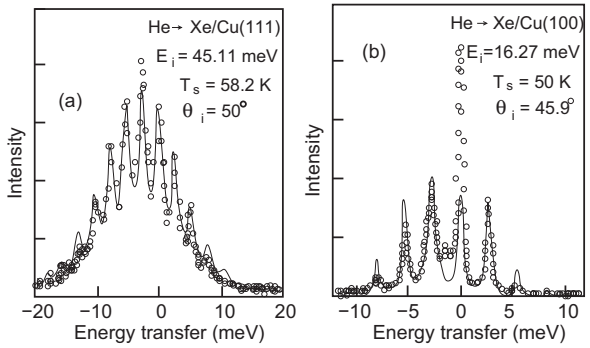

(**a**) He→Xe/Cu(111) scattering,
(**b**) He→Xe/Cu(100) scattering.
Circles: experiment;
solid line: theory (exponentiated distorted-wave Born approximation).
(A. Siber *et al.*, PRB **59**, 5898 (1999))

Dispersionless collective Xe vibrational modes

Atomic and molecular adsorption

Sticking probability

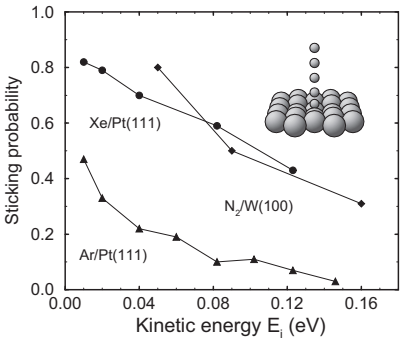

A. Zangwill, Physics at Surfaces

Discussion

Sticking or trapping probability decreases with increasing kinetic energy

$P_E(\epsilon)$ probability that an incoming particle with kinetic energy E will transfer the energy ϵ to the surface

$\Rightarrow$ atomic or molecular sticking probability:

$$S(E) = \int_E^{\infty} P_E(\epsilon)\, d\epsilon, \qquad (180)$$

Energy has to be transferred to substrate excitation, i.e., either phonons or electron-hole pairs.

$\Rightarrow$ Dissipation needed in any theoretical description

Hard-cube model of atomic adsorption

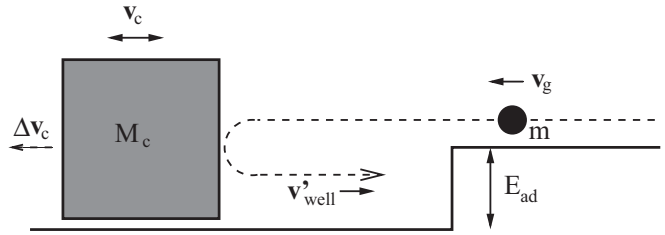

Trapping probability

$$P_{\rm trap}(v_{\rm g}) = \frac{1}{2} + \frac{1}{2}{\rm erf}(\alpha v_{\rm lim}) + \frac{\exp\left\{-(\alpha v_{\rm lim})^2\right\}}{2\sqrt{\pi}\alpha v_{\rm well}} \quad \text{with } \alpha = \sqrt{M_c/2k_{\rm B}T_{\rm s}} \qquad (181)$$

$$v_{\rm well} = -\sqrt{v_{\rm g}^2 + \frac{2E_{\rm ad}}{m}}\,; \quad v_{\rm lim} = \frac{\mu+1}{2}\sqrt{\frac{2E_{\rm ad}}{m}} - \frac{\mu-1}{2}v_{\rm well} \quad \text{with } \mu = m/M_c \qquad (182)$$

Sticking probability in the hard-cube model

Sticking probability

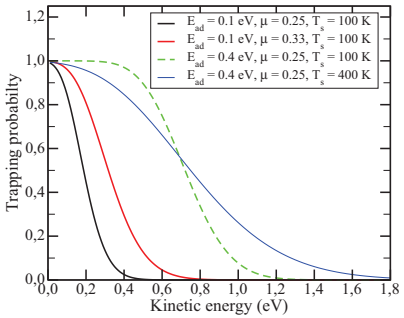

Hard-cube model calculations

Discussion

Sticking or trapping probability decreases with increasing kinetic energy

Larger energy transfer to substrate with increasing mass of the incoming atom and with larger well depth

Temperature corresponds to an averaging which leads to a decrease for negative curvature and an increase for positive curvature of the sticking curve

$E \to 0 \quad \Rightarrow \quad S(E) \to 1$
Classical limit

Quantum limit: $S(E) \to S_0 < 1$

Quantum effects in the sticking of rare gas atoms on Ru(0001)

H. Schlichting, D. Menzel, T. Brunner, and W. Brenig, J. Chem. Phys. **97**, 4453 (1992).

Sticking probability

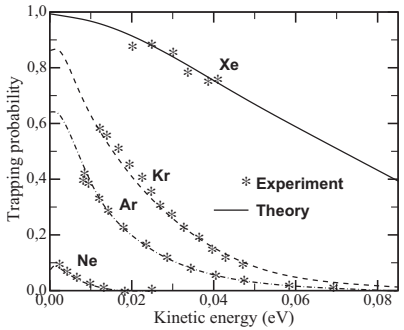

Forced-oscillator model

Forced-oscillator model

Surface modeled by an ensemble of quantum surface oscillators with a Debye spectrum

Scattered particle treated classically
→ trajectory approximation

Calculations yield the energy distribution of excited phonons → $P_E(\epsilon)$

Quantum probability for elastic scattering ($\Delta E = 0$) leads to

$S(E) \to S(E \to 0) = S_0 < 1$

for lighter rare gases

Dissociative adsorption

Dissociative adsorption event

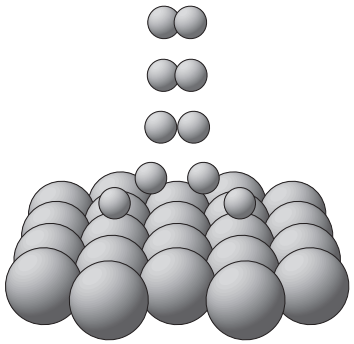

Discussion

Dissociation: further channel for energy transfer:
Conversion of center-of-mass kinetic energy into kinetic energy of the fragments relative to each other

Dissociation of light molecules like H_2 on a heavy substrate:

Energy transfer to substrate degrees of freedom negligible

Sticking probability entirely determined by dissociation probability

Dissociative adsorption can be described within low-dimensional potential energy surface for fixed substrate atoms

Vibrationally enhanced dissociative adsorption

Schematic trajectories

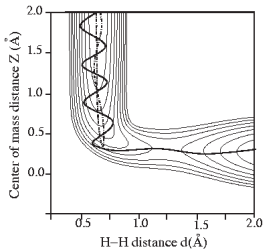

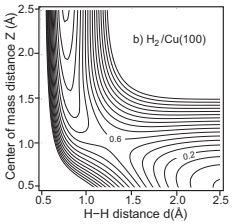

Discussion

Late barrier system:

Barrier after curved region of PES

Vibrational motion very effective for overcoming barrier to dissociation

⇒ *Vibrationally enhanced dissociation*

Efficiency of vibrationally enhanced dissociation depends on the curvature of the reaction path

Discussion

Calculated elbow plot using GGA-DFT

S. Sakong and A. Groß, Surf. Sci. **525**, 107 (2003)

Curvature smaller than in the model PES

Vibrationally adiabatic effects also important (see below)

Dissociative adsorption probability for H_2/Cu

Dissociative adsorption probability

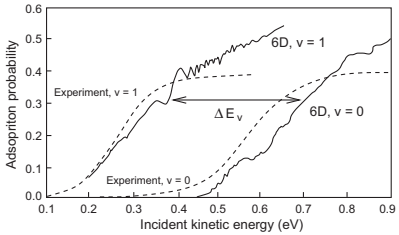

Sticking probability for $v = 0$ and $v = 1$ initial vibrational states. Exp.: H.A. Michelsen and D.J. Auerbach, JCP **94**, 7502 (1991), Theory: D.A.McCormack *et al.*, CPL **328**, 317 (2000).

Discussion

H_2 dissociative adsorption on Cu activated

Strong enhancement of the sticking probability for vibrationally excited H_2 molecules

Vibrational efficacy:

$$\chi = \frac{\Delta E_0}{\hbar\omega_{\rm vib}} \qquad (183)$$

$\chi \approx 0.6$ in the figure

Dissociative adsorption of H_2 on Pd(100)

Elbow plots

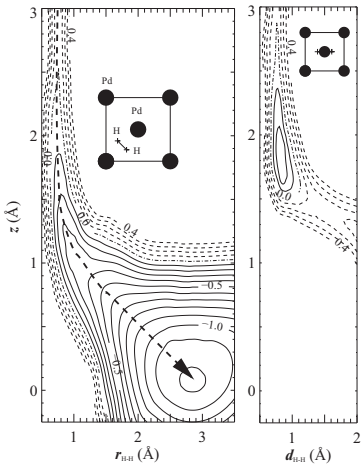

S. Wilke and M. Scheffler, PRB 53, 4926 (1996).

Nonactivated adsorption

On Pd(100), hydrogen dissociates spontaneously along reaction paths without any barrier.

PES depends strongly on the lateral coordinates and the orientation of the hydrogen molecule:

PES highly corrugated and anisotropic

Far away from the surface: H_2 molecule first attracted to the on-top site:

corresponds to dihydride form of PdH_2

In general, chemisorbed molecular states not stable on metal surfaces, H_2 rather dissociates

Sticking probability of H_2 on Pd(100)

Comparison theory-experiment

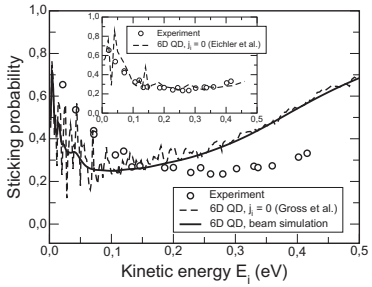

Exp.: K.D. Rendulic *et al.*, Surf. Sci. **208**, 404 (1989), Theory: A. Groß *et al.*, PRL **75**, 2718 (1995).

Steering effect

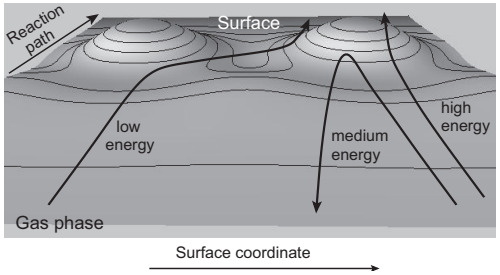

All *six* hydrogen degrees of freedom treated quantum dynamically

Initial decrease in $S(E_i)$ caused by the suppression of the steering effect

Oscillations quantum effect: opening of new scattering channels with increasing energy

Steering effect

Schematic trajectories

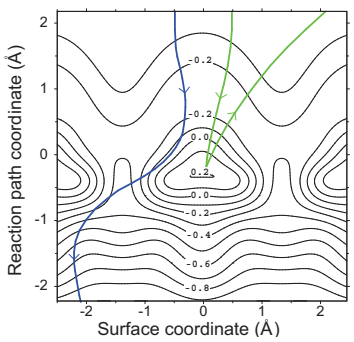

Steering

- PES has activated as well as non-activated paths towards dissociative adsorption
- Low energies: effective steering and reorientation of the molecules towards favorable configurations for dissociation
- Larger energies: steering suppressed
- Even larger energies: direct propagation over barriers

Molecular Dynamics Snapshots of H_2 Impinging on Pd(100)

Steering effect: Efficient aligning at low kinetic energies ($E_i = 0.01$ eV)

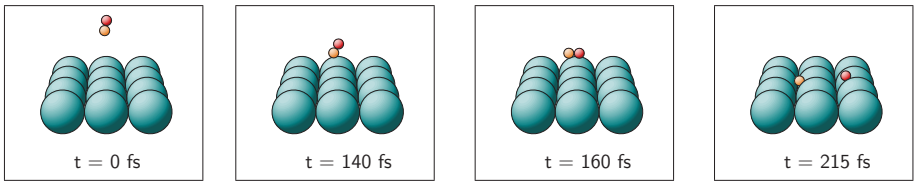

At higher kinetic energies: Steering is no longer effective ($E_i = 0.12$ eV)

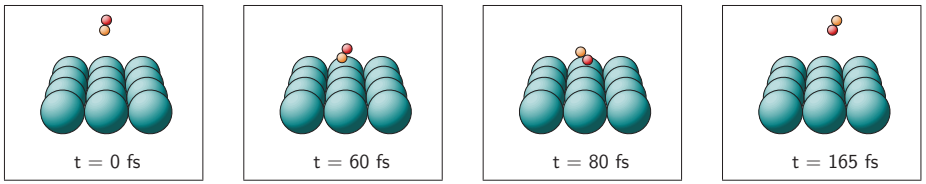

Vibrational effects for H_2/Pd(100)

Dissociative adsorption probability

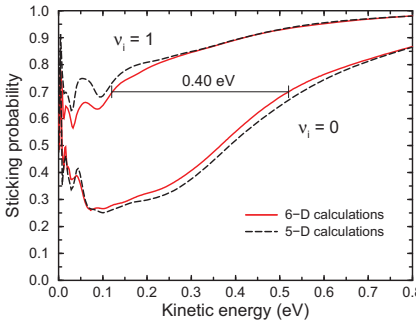

Sticking probability for $v = 0$ and $v = 1$ initial vibrational states

Discussion

Enhancement of the sticking probability for vibrationally excited H_2 molecules

Vibrational efficacy $\chi = \frac{\Delta E_0}{\hbar\omega_{\rm vib}} \approx 0.8$

Vibrational effects reproduced in 5-D vibrationally adiabatic calculations

⇒ Curvature of the reaction path cannot be responsible for vibrational effects

Vibrationally adiabatic potentials

Potential along the reaction path

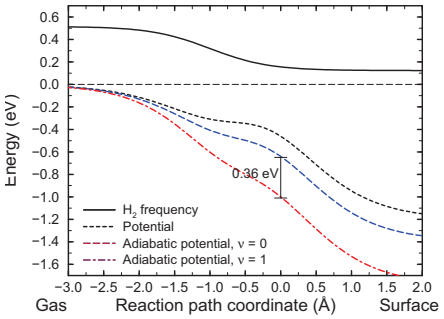

Vibrational frequency and vibrationally adiabatic potententials along the minimum energy path

Discussion

Vibrational adiabatic 5-D results close to 6-D results:

⇒ *Vibrational adiabatic potentials*

$$V^{\nu}_{adia}(s) = V_o(s) + (\hbar\omega(s) - \hbar\omega_{gas})\,(\nu + \frac{1}{2}). \quad (184)$$

Lowering of the frequency upon adsorption ⇒ lowering of vibrationally adiabatic potentials

Barriers become effectively smaller for vibrating molecules

⇒ Higher sticking probability

Vibrational effects in desorption

Vibrational temperatures

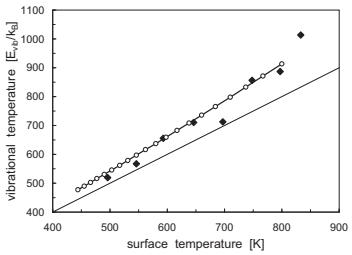

Exp.: ◇, theory: ○

D. Wetzig *et al.*, Phys. Rev. B **63**, 205412 (2001).

Discussion

Adsorption probabilities related to desorption via time invariance

$$D_n(E_\perp) = \frac{1}{Z}\, S_n(E_\perp)\, e^{-\frac{E_n+E_\perp}{k_B T_s}}. \quad (185)$$

$E_\perp$ perpendicular kinetic energy ,
n index characterizing the internal state

Mean vibrational energy characterized through vibrational temperature
$T_{\rm vib} = \langle E_{\rm vib}\rangle / k_B$

Vibrational enhancement in adsorption
⇔ Vibrational heating in desorption

Rotational effects in desorption

Rotational temperatures

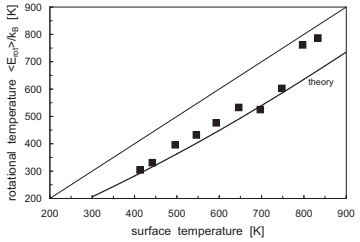

Exp.: boxes, theory: solid line

D. Wetzig *et al.*, Phys. Rev. B **63**, 205412 (2001).

Discussion

Rotational temperature
$T_{\rm rot} = \langle E_{\rm rot}\rangle / k_B$

Rotational cooling in desorption
⇒ Rotational hindering in adsorption

Rotational temperature corresponds to an average over all rotational quantum numbers

⇒ no microscopic information

Rotational effects in the adsorption of D_2/Cu(111)

Detailed balance: Desorption flux ⇔ Adsorption probability

$$f(t,\theta_i,v,j)dt \;=\; K_t \left(\frac{x}{t'}\right)^4 \exp\left(-\frac{E_i}{k_B T_s}\right) \cos\theta_i \; S_0(E_i,\theta_i,v,j)dt \quad (186)$$

Adsorption probabilities

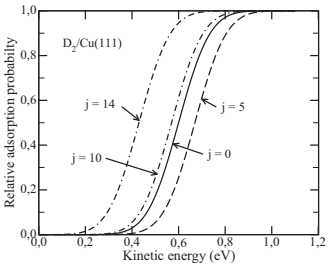

Adsorption probability for D_2/Cu(111) derived from desorption experiments

H.A. Michelsen *et al.*, J. Chem. Phys. **98**, 8294 (1993).

Discussion

Sticking probability derived from the state-resolved desorption flux

Width of sticking curve independent of j

Low j ⇒ rotational hindering

High j ⇒ rotational enhancement

Rotational hindering

Schematic trajectory

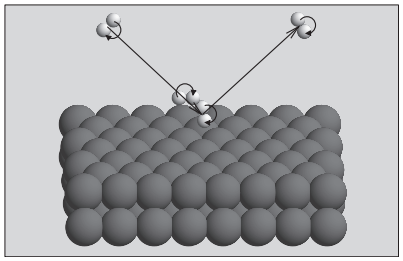

Rotating molecule scattered at a (111) surface

Rotational hindering

Molecular axis has to be parallel to the surface for dissociation

Rotating molecule:

Molecule will rotate out of favorable orientation for dissociation during the collision process

⇒ rotating molecule will be scattered back into the gas phase

Orientation of rotational axis

Rotating molecules

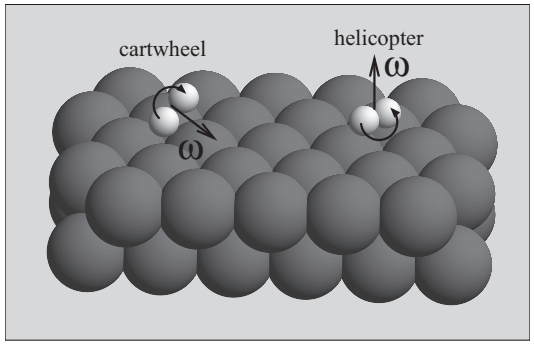

Orientation

Classical:

$\vec{\omega} \parallel \vec{\hat{z}}$: helicopter rotation

$\vec{\omega} \perp \vec{\hat{z}}$: cartwheel rotation

Quantum:

$m = j$: helicopter rotation

$m = 0$: cartwheel rotation

Helicopter molecules have their axis already parallel to the surface which is favorable for dissociation while cartwheel molecules have a high probability to hit the surface in the unfavorable upright orientation

Rotational effects in the adsorption of H_2/Pd(100)

Sticking probability

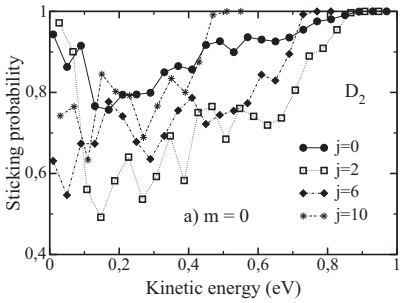

Sticking probability for cartwheel molecules
Arezoo Dianat and Axel Groß, Phys. Chem. Chem. Phys. **4**, 4126 (2002).

Discussion

Non-monotonous behavior of the sticking probality as a function of the rotational quantum number in 3D quantum calculations

Rotational enhancement

⇒Rotational adiabatic potential:

$$V^j_{adia}(s) = V_o(s) + \frac{\hbar^2 j(j+1)}{2\mu}\left(\frac{1}{r^2_{eq}} - \frac{1}{r(s)^2}\right)$$

Bond length increases upon dissociation

⇒ lowering of rotational quantum energy

Barriers become effectively smaller for rotating molecules

⇒ Higher sticking probability

Test of rotational adiabatic effects

Sticking probability

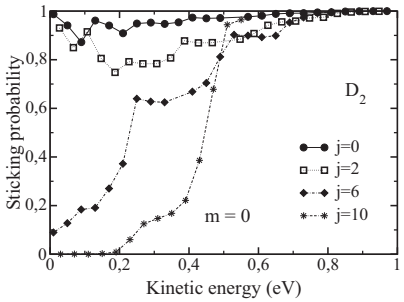

Sticking probability for cartwheel molecules with a fixed bond length
Arezoo Dianat and Axel Groß, Phys. Chem. Chem. Phys.

Discussion

The D-D bond length and consequently the D_2 moment of inertia are kept frozen at their gas phase values

Increasing the rotational quantum number now leads to a further suppression of the sticking probability

⇒ Confirmation that change of bond length causes rotational enhancement of the sticking probability

Note that the sticking probability for $j = 0$ increases for the fixed bond length
Classical explanation: Re-orientation easier for shorter bond length

Adsorption probability for helicopter molecules

Sticking probability

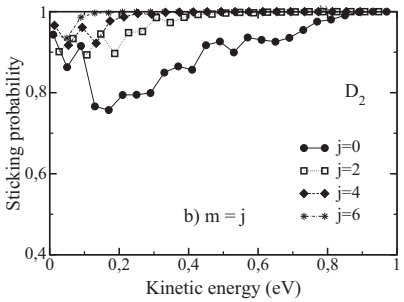

Sticking probability for helicopter molecules

Discussion

Sticking probability larger for helicopter than for cartwheel molecules ⇒ steric effect

Sticking probability increases with rotational quantum number
Combination of steric and adiabatic effects

Steric effects in adsorption should be related to desorption properties
Rotational alignment

Rotational alignment in desorption

Alignment

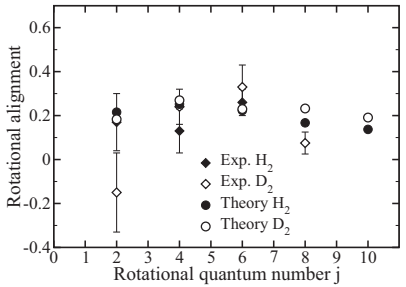

Measured and calculated rotational alignment for a surface temperature of $T_s = 700$ K
Exp.: D. Wetzig *et al.*, Surf. Sci. **402**, 232 (1998);
Theory: A. Dianat and A. Groß, Phys. Chem. Chem. Phys. **4**, 4126 (2002).

Discussion

$$A_0^{(2)} = \langle J_i | \frac{3m^2 - J^2}{\vec{J}} | J_i \rangle \quad (187)$$

Alignment parameter range

$$-1 \leq A_0^{(2)} \leq 2 \quad (188)$$

Preferential population in desorption:

$A_0^{(2)} \leq 0$: cartwheel

$A_0^{(2)} > 0$: helicopter

Positive alignment in desorption ⇔ parallel orientation favorable for dissociation

Non-monotonous behavior ⇔ Rotationally adiabatic effects reduce difference between cartwheel and helicopter dissociation

Quantum sticking probability H_2/Pd(110)

A. Dianat and A. Groß, J. Chem. Phys. **120**, 5339 (2004)

Six-dimensional quantum dynamical study on a parametrized PES based on DFT calculations by Ledentu *et al.*, Surf. Sci. **412**, 518 (1998).

Cartwheel rotations

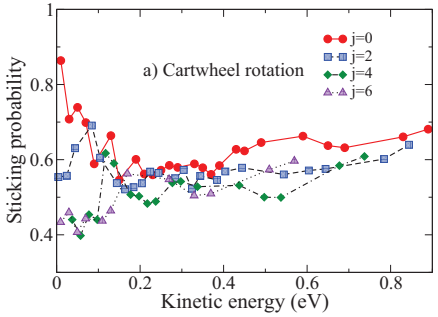

Helicopter rotations

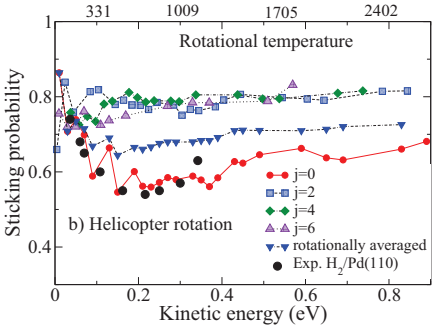

Experiment: C. Resch *et al.*, Surf. Sci. **316**, L1105 (1994)

H_2/Pd(110): orientational effects

A. Dianat and A. Groß, J. Chem. Phys. **120**, 5339 (2004)

Sticking for $j = 3, m$ molecules

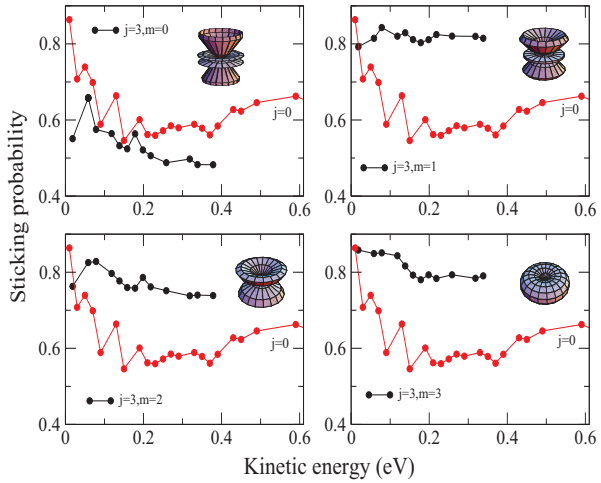

Rotational hindering only for $j = 3, m = 0$ molecules, but rotational enhancement for $j = 3, m \geq 1$ molecules

Interpretation:

Strong washboard-like corrugation of the (110) surface leads to enhanced dissociation for off-normal orientation of the molecular axis

H_2/Pd(110): Rotational heating in desorption

A. Dianat and A. Groß, J. Chem. Phys. **120**, 5339 (2004)

Rotational temperatures

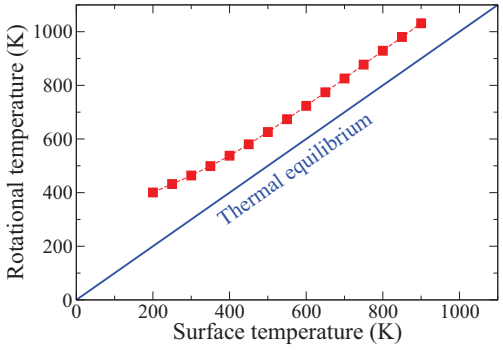

Unusual rotational heating in the thermal desorption of H_2/Pd(110) predicted

Rotational heating consequence of the strong steric effects in the dissociation dynamics of H_2/Pd(110)

Molecular beam experiments: H_2 and D_2 on Rh(111)

M. Beutl, J. Lesnik and K. D. Rendulic, Surf. Sci.. **429**, 71 (1999)

Sticking coefficient

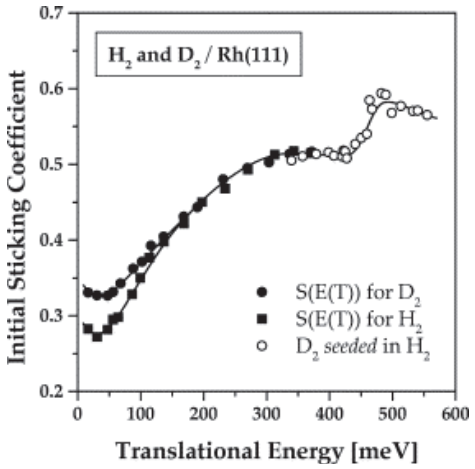

Low kinetic energies: non-activated behavior of dissociative adsorption (steering)

Remarkable feature: step in the dissociative adsorption probability at $E_{\mathrm{kin}} \approx 0.45$ eV

Interpretation: Opening up of additional dissociation channel at high kinetic energies

Ab initio PES of H_2/Rh(111)

A. Dianat, S. Sakong and A. Groß, to be published

Potential energy surface of H_2/Rh(111) determined with DFT-GGA calculations

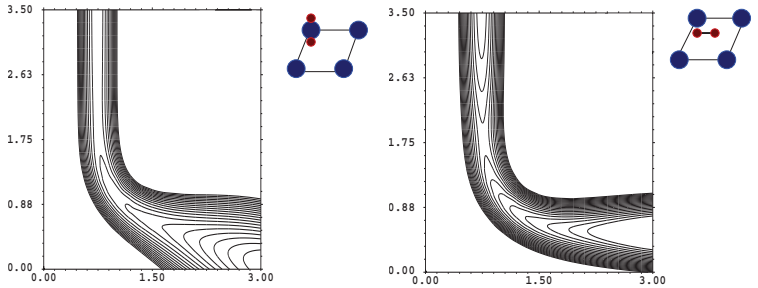

H-H distance (Å)

Only few non-activated paths towards dissociative adsorption

Early barrier system: barriers almost independent of azuimuthal orientation of H_2 ⇒ 5D PES

No indication for additional dissociation channel at higher kinetic energies

Quantum sticking probability H_2/Rh(111)

A. Dianat, S. Sakong and A. Groß, to be published

5D quantum sticking probability on parametrized PES

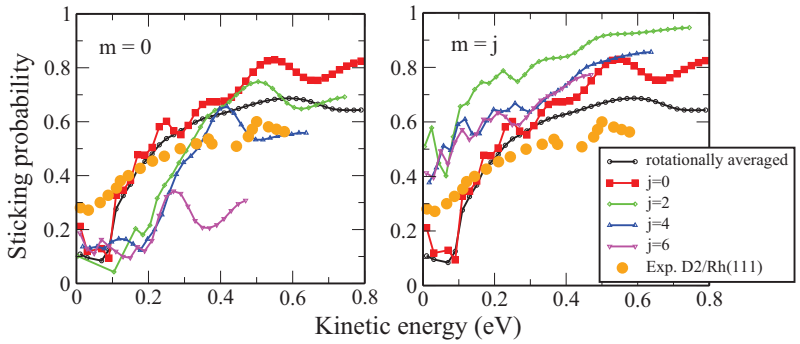

Bump in sticking probability at $E_{\mathrm{kin}} \approx 0.45$ eV reproduced in calculation for $j = 0$ although no additional adsorption channel opens up

⇒ Dynamical effect ?

Car exhaust catalyst

Structure of the catalyst

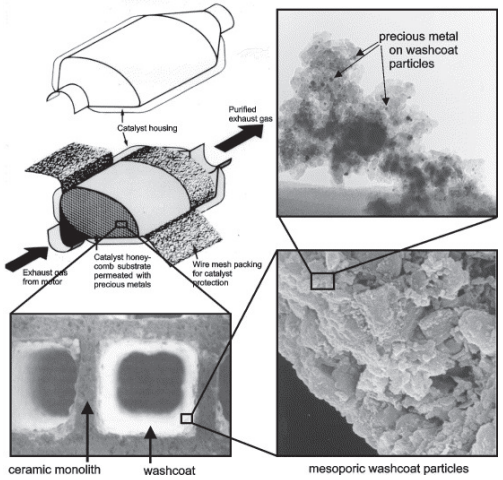

H.-J. Freund, Surf. Sci. **500**, 271 (2002)

Elementary steps in CO oxidation

Schematic animation of CO oxidation
(C.Stampfl, FHI Berlin)

Adsorption of O_2/Pt(111)

Dissociation of O_2/Pt(111)

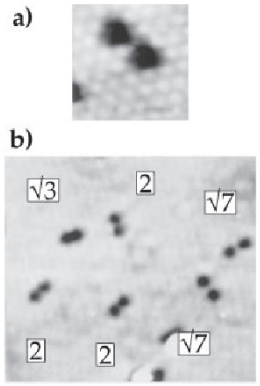

STM images of the dissoziation of O_2 on Pt(111) ($T_s \sim 160$ K) (Wintterlin *et al.*, PRL **77**, 123 (1996)).

Experimental results

- O_2/Pt(111) well-studied experimentally (see, e.g., Wurth *et al.*, PRL **65**, 2426 (1990)); still the molecular adsorption process is not fully understood
- Two molecular chemisorption states
- $T_s \gtrsim 100$ K: O_2 dissociates on Pt(111). STM: mean distance of atomic fragments two lattice units
- Molecular beam experiments ($T_s \lesssim 100$ K): O_2 does not dissociate, even at kinetic energies of up to 1.4 eV

Sticking probability O_2/Pt(111)

Sticking probability

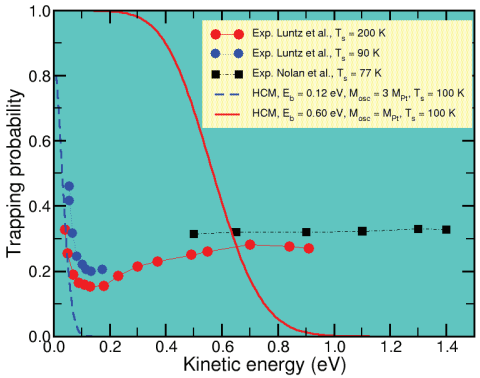

Experiment: Luntz *et al.*, JCP **89**, 4381 (1988), Nolan *et al*, JCP **111**, 3696 (1999).

Hard cube model

Blue: $E_\mathrm{b} = 0.12$ eV, $m_{osc} = 3 \cdot m_\mathrm{Pt}$, $T_\mathrm{s} = 100$ K
Red: $E_\mathrm{b} = 0.60$ eV, $m_{osc} = 1 \cdot m_\mathrm{Pt}$, $T_\mathrm{s} = 100$ K

Interpretation of the experimental data

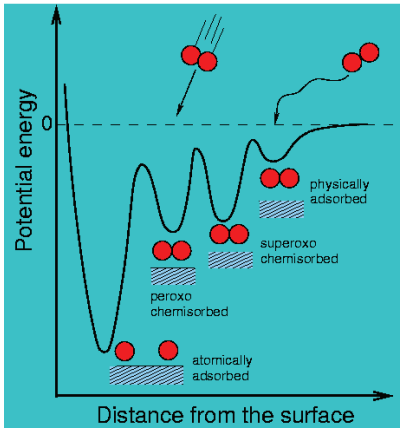

After Nolan *et al.*, JCP **111**, 3696 (1999).

Molecular adsorption dynamics: O_2/Pt(111)

A. Groß, M. Scheffler, M.J. Mehl, and D.A. Papaconstantopoulos, Phys. Rev. Lett. **82**, 1209 (1999)
A. Groß, A. Eichler, J. Hafner, M.J. Mehl, and D.A. Papaconstantopoulos, subm. to Phys. Rev. Lett.

Molecular adsorption dynamics:
energy transfer to the substrate and energy dissipation have to be taken into account
$\Rightarrow$ Tight-binding parametrization of the O_2/Pt(111) potential energy surface

top-bridge-top orientation

bridge-hcp-top orientation
molecular axis slightly canted

bridge-top-bridge orientation

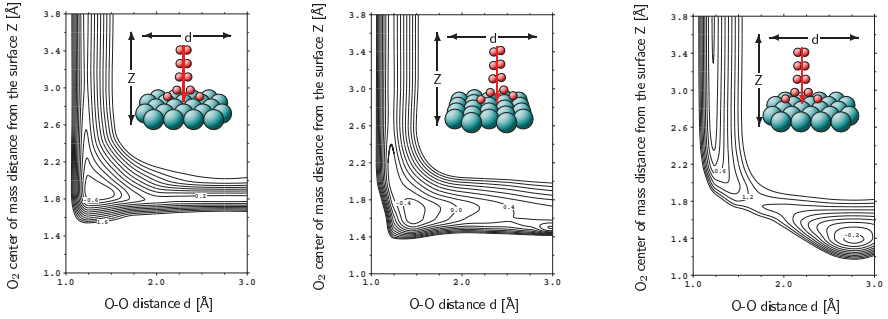

Tight-binding molecular dynamics simulations: O_2/Pt(111)

Simulation cell

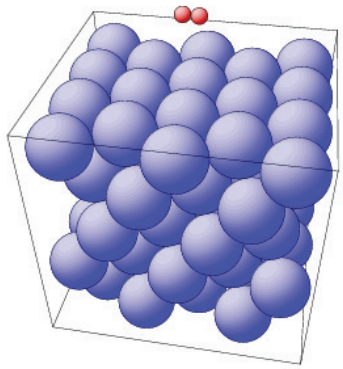

5 layers of a c(4×4) Pt(111) surface plus O_2 molecule

Technical details

- Simulations performed in a 5 layer c(2×4) cell ($E_\mathrm{kin} \leq 0.3$ eV) or in a c(4×4) cell ($E_\mathrm{kin} \geq 0.4$ eV), respectively. All atoms except for the Pt bottom layer are treated dynamically
- Time step of the TBMD simulations 1 fs, simulation time per trajectory ≤ 2 ps
- Sticking probabilities determined by averaging over 150 trajectories per energy with random initial conditions
  $\Rightarrow$ statistical uncertainty of reaction probabilities $\pm$ 0.07

Tight-binding molecular dynamics simulations: O_2/Pt(111)

A. Groß, A. Eichler, J. Hafner, M.J. Mehl, and D.A. Papaconstantopoulos, subm. to Phys. Rev. Lett.

Sticking probability

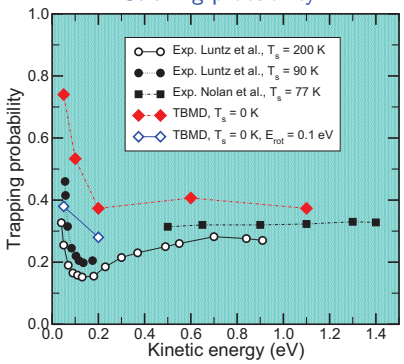

Comparison of calculated and measured sticking probability as a function of the kinetic energy

Over the whole energy range sticking probability is determined by the trapping into the molecular chemisorption states

Dissociation?

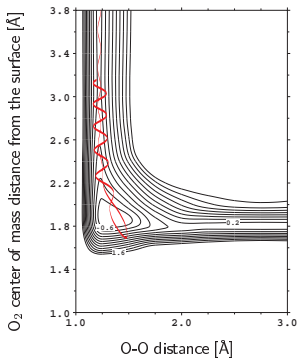

Projection of a trajectory of a O_2 molecule onto the Zd plane, initial kinetic energy $E_{\mathrm{kin}} = 0.6$ eV

O_2 molecules do not directly dissociate on Pt(111) because of steric hindrance
$\rightarrow$ dissociation of O_2/Pt(111) is a two-step process involving thermalisation

Steering mechanism O_2/Pt(111): snapshots

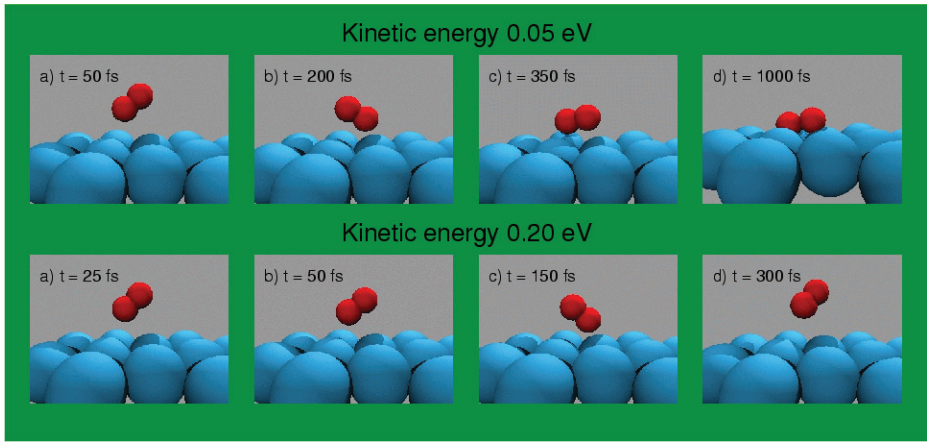

At low energies, trapping probability is not given by the energy transfer to the substrate *per se*, but rather by the probability to enter the molecular adsorption well

Steering: At low energies, molecules with an unfavorable configuration for adsorption will be very efficiently steered towards the molecular adsorption well

Steering mechanism O_2/Pt(111): animation

$E_{\mathrm{kin}} = 0.05$ eV

Calculated TBMD trajectory with an initial kinetic energy of $E_{\mathrm{kin}} = 0.05$ eV

$E_{\mathrm{kin}} = 0.2$ eV

Calculated TBMD trajectory with an initial kinetic energy of $E_{\mathrm{kin}} = 0.2$ eV

Steering: At higher kinetic energies steering will be effectively suppressed:

$\Rightarrow$ strong decrease of the sticking probability

High Energies: Dynamical Precursor

$E_{\mathrm{kin}} = 1.1$ eV

Calculated TBMD trajectory with an initial kinetic energy of $E_{\mathrm{kin}} = 0.2$ eV

Energy redistribution

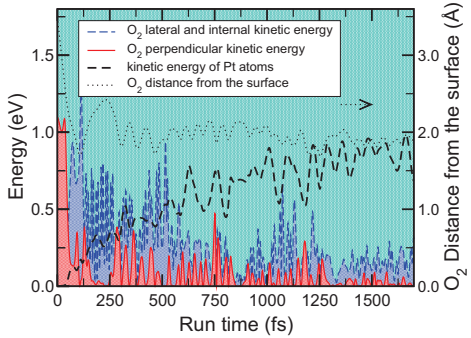

Energy redistribution during the run time of the trajectory

Energy transfer of the impinging molecule into lateral and internal degrees of freedom $\Rightarrow$ Trapping into a dynamical precursor state

Lateral distribution of adsorbed O_2 molecules

Simulation unit cell

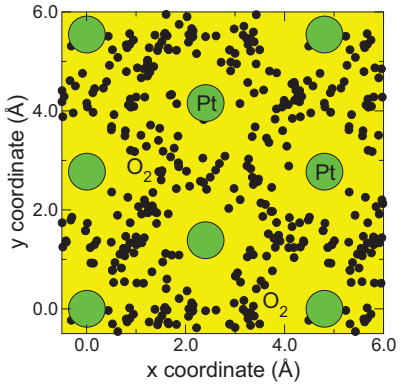

Lateral positions of the O_2 center of mass upon adsorption for kinetic energies $\lesssim 0.2$ eV

Discussion

Center of mass positions of the O_2 molecules plotted as a function of the lateral coordinate in the surface unit cell
Note that the O_2 molecules are still not fully equilibrated
$\Rightarrow$ Molecules not exactly at their local equilibrium positions

Molecular precursors at the bridge, the fcc hollow and the hcp hollow approximately equally populated

Top position unfavorable for adsorption

Dependence of trapping probability on angle of incidence

A. Groß, A. Eichler, J. Hafner, M.J. Mehl, and D.A. Papaconstantopoulos, subm. to Phys. Rev. B

$E_{\mathrm{kin}} = 0.3$ eV

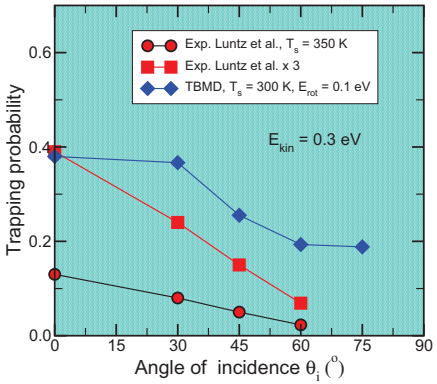

$E_{\mathrm{kin}} = 1.1$ eV

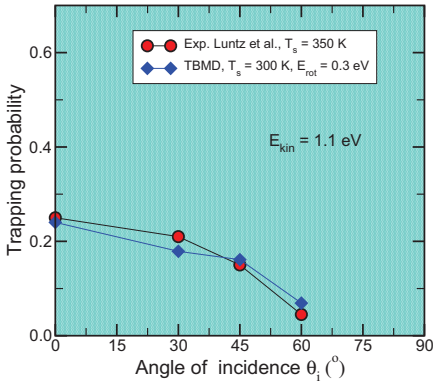

Strong decrease of the trapping probability for larger angle of incidence
No normal energy scaling
$\Rightarrow$ Significant role of surface corrugation in the adsorption process

Scattering of O_2/Pt(111)

$E_{\mathrm{kin}} = 1.1$ eV, $\theta_i = 45°$

Calculated TBMD trajectory

$E_{\mathrm{kin}} = 1.1$ eV, $\theta_i = 60°$

Calculated TBMD trajectory

Scattering: molecules in a parallel configuration get closer to the surface than molecules in an upright orientation

Angular distribution in scattering

Scattering distribution

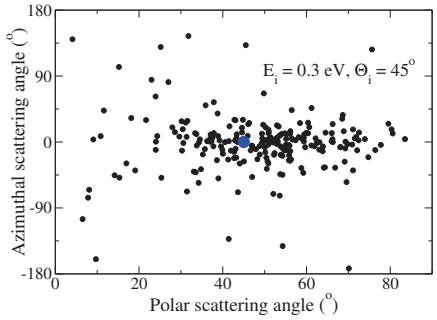

Inplane scattering

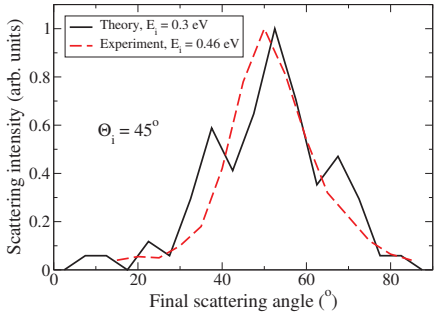

Exp.: A.E. Wiskerke *et al.*, Surf. Sci. **272**, 256 (1992).

Scattering mostly along the incident direction $\rightarrow$ inplane scattering
Calculated inplane scattering distribution somewhat broader which might be caused by the insufficient statistics

Angular distribution in scattering

Scattering distribution

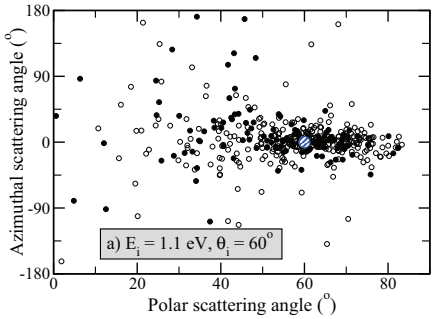

Inplane scattering

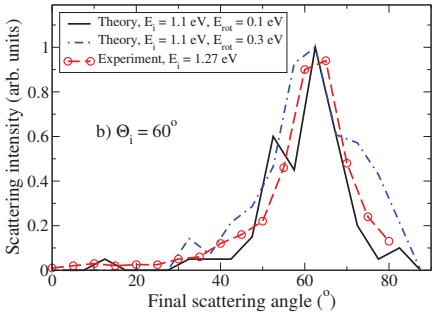

Exp.: A.E. Wiskerke *et al.*, Surf. Sci. **272**, 256 (1992).

Scattering distribution of O_2/Pt(111) similar to Ar/Pt(111)

⇒ Broadening of scattering distribution can be explained by the energy transfer to a vibrating flat surface

Energy transfer in scattering

Mean energy transfer

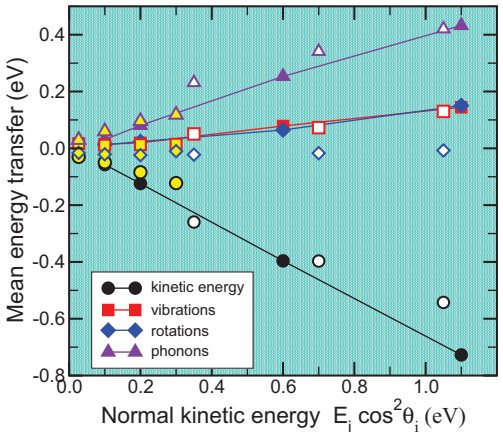

Normal energy scaling

Yellow-filled symbols:
$E_{\rm kin} = 0.3$ eV, $E_{\rm rot} = 0.1$ eV, $T_s = 300$ K

White-filled symbols:
$E_{\rm kin} = 1.1$ eV, $E_{\rm rot} = 0.3$ eV, $T_s = 300$ K

Phonons main energy loss channel

Normal energy scaling approximately obeyed

Exception: Energy transfer to rotations, scattering rotationally elastic for initially rotating molecules

Corrugated of flat surface?

Normal incidence

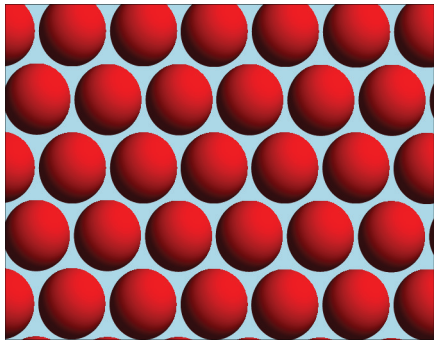

Grazing incidence

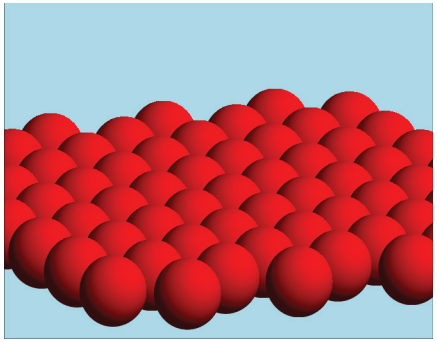

Non-normal incidence leads to shadowing effects and averaging over surface unit cell

Kinetic modelling of processes on surfaces

For many processes on surfaces such as diffusion the time between two successful events is in the order of nanoseconds or even longer

Molecular dynamics simulations calculate all unsuccessful events explicitly
⇒ time scale in MD runs typically limited to picoseconds

Kinetic approach neccessary

Rate of a microscopic process

$$k = \frac{k_B T}{h} \exp\left(-\frac{\Delta F}{k_B T}\right) \quad \text{with} \quad \Delta F = E_a - T\Delta S \tag{189}$$

ΔF difference in free energy

$$\Rightarrow k = k_0 \exp\left(-\frac{E_a}{k_B T}\right) \quad \text{with} \quad k_0 = \frac{k_B T}{h} \exp\left(\frac{\Delta S}{k_B}\right) \tag{190}$$

Flux in the transition state theory

Potential with two states:

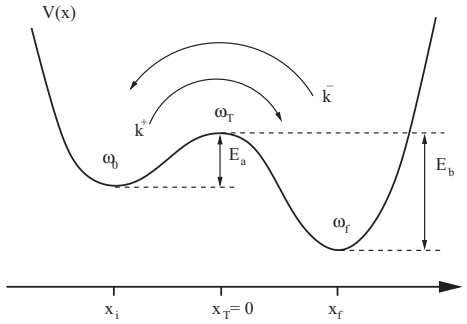

Rate at the transition state $x = 0$:

Equilibrium average of the one-way flux at the transition state

$$k_{\rm TST} = \frac{\langle \delta(x)\ \dot{x}\ \Theta(\dot{x})\rangle}{\langle \Theta(-x)\rangle} \tag{191}$$

Transition state theory

1-D Potential with two states

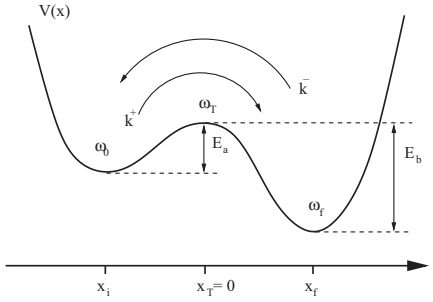

1-D TST

Equilibrium one-way flux at the TS $x = 0$:

$$k_{\rm TST} = \frac{\langle \delta(x)\ \dot{x}\ \Theta(\dot{x})\rangle}{\langle \Theta(-x)\rangle} \tag{192}$$

$$= Z_0^{-1}\frac{1}{2\pi\hbar}\int dqdp\,\delta(q)\dot{q}\theta(\dot{q})\,e^{-\beta H(q,p)} \tag{193}$$

$$\approx \frac{\omega_0}{2\pi}\ \exp(-\beta E_a) \tag{194}$$

ω_0: attempt frequency

Normal-mode frequency hard to calculate ⇒ often guessed

Typical value: $\omega_0 \approx 10^{13}$ s^{-1}

Multidimensional transition state theory

Multi-dimensional result

Nonlinear coordinate coupled to N harmonic vibrations

$$k_{\rm TST} = \frac{k_BT}{h}\frac{Z^{\rm TS}}{Z_0}\ \exp(-\beta E_a)$$

$$= \frac{1}{2\pi}\frac{\prod_{i=0}^{N}\omega_i^{(0)}}{\prod_{i=1}^{N}\omega_i^{\rm TS}}\exp(-\beta E_a) \tag{195}$$

$\omega_i^{(0)}$ and $\omega_i^{\rm TS}$ normal-mode eigenvalues at the initial well and the transition state.

In principle, all variables in (195) can be evaluated by DFT calculations

However, usually the determination of eigenmode-frequencies is computationally very demanding so that the prefactor in (195) often just estimated

Arrhenius behavior

TST rate can be reformulated employing the Helmholtz free energy F

$$Z = \exp[-(E - TS)/(k_BT)]$$
$$= \exp[-F/(k_BT)] \tag{196}$$

$$\Rightarrow k_{\rm TST} = \frac{k_BT}{h}\exp\left(\frac{\Delta S}{k_B}\right)\ \exp\left(-\frac{E_a}{k_BT}\right)$$
$$= k_0\ \exp\left(-\frac{E_a}{k_BT}\right)\ , \tag{197}$$

where $\Delta S = S_{\rm TS} - S_0$ is the entropy change.

Eq. (197) corresponds to Arrhenius expression.

Note: k_0 temperature dependent

Kinetic treatment of rare events

Molecular dynamics: simulation of many unsuccessful events

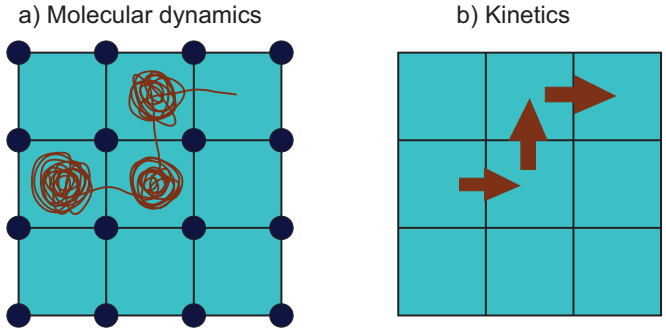

Schematic sketch of difference between dynamical and kinetic simulation of diffusion

Kinetic Monte Carlo: Coarse-grained, lattice-based atomistic simulation technique

Kinetic Monte Carlo

1) Determination of all processes with rate k_i that are possible for a given configuration

2) Calculation of the total rate $R = \sum_i k_i$

3) Choose two random numbers ρ_1 and ρ_2 in the range (0,1].

4) Find the integer number l for which

$$\sum_{i=0}^{l-1} k_i \;\leq\; \rho_1 R \;<\; \sum_{i=0}^{l} k_i$$

5) Execute process l.

6) Update the simulation time $t = t + \Delta t$ with $\Delta t = -\ln(\rho_2)/R$.

7) Proceed with step 1).

Simulation of processes on larger time and length scales: Kinetic Monte Carlo Algorithm

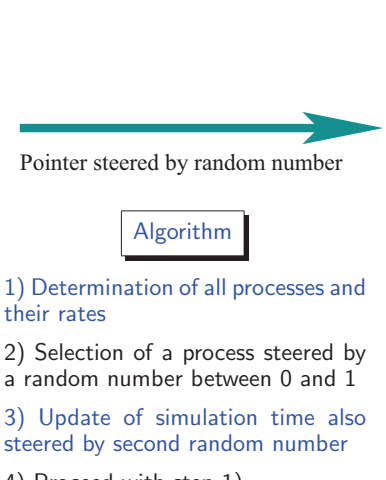

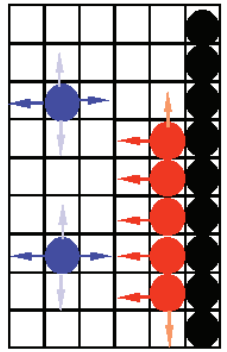

Algorithm

1) Determination of all processes and their rates

2) Selection of a process steered by a random number between 0 and 1

3) Update of simulation time also steered by second random number

4) Proceed with step 1).

Peter Kratzer, FHI Berlin

Distance of oxygen atoms after dissociation

O-O distances determined by kinetics or dynamics?

Experiment

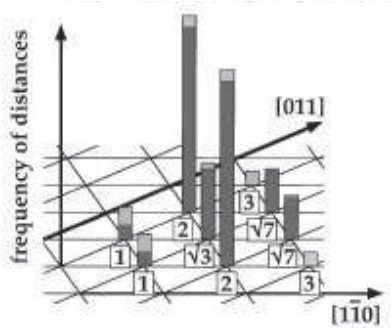

(Wintterlin *et al.*, PRL **77**, 123 (1996))

kMC Simulation

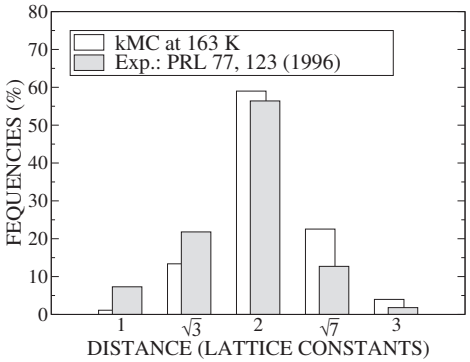

O-O distance distribution can only approximately be reproduced in kMC simulations with unrealistic barrier heights
⇒ Distribution determined by dynamics

Kinetics of O_2/Pt(111) adsorption and desorption

Animation

Ab initio based kinetic Monte Carlo simulation of the adsorption and desorption of O_2/Pt(111)

TPD spectrum

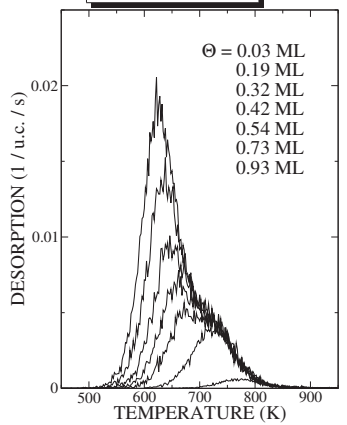

Calculated TPD spectrum
C. Sendner and A. Groß, JCP **127**, 014704 (2007).

Molecular and dissociative adsorption and desorption as a function of the surface temperature

Formation of O_2 chains

Exp.: T. Zambelli *et al.*, Nature **390**, 495 (1997); theory: C. Sendner and A. Groß, JCP **127**, 014704 (2007).

Experiment

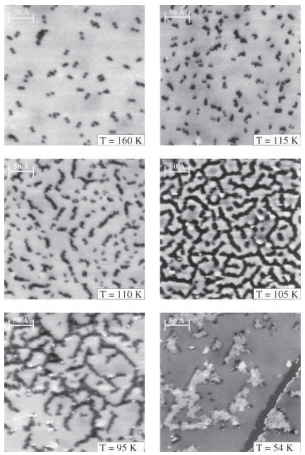

kMC Simulation

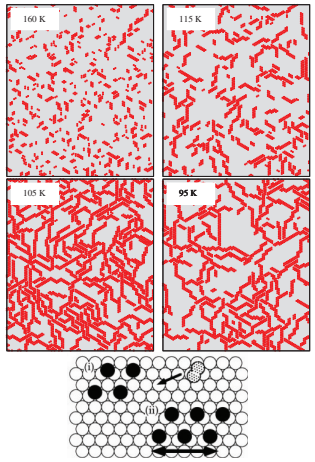

Chain formation caused by lowered dissociation barriers in the vicinity of O atoms

Ab initio kMC: Water adsorption on Pd(111)

S.K. Desai, V Pallassana, and M. Neurock, J. Phys. Chem. B **105**, 9171 (2001)

Neurock group home page

Ab initio derived kinetic Monte Carlo simulation of the adsorption of water on Pd(111) at 0°C and 1 atm

Obviously no icelike-structure included in the kMC structure list
$\Rightarrow$ no formation of water bilayer in the simulation

Kinetic lattice gas model

Description of surface processes on a mesoscopic length and time scale:

Lattice gas Hamiltonian

$$H(\{\vec{R}\}) = \sum_{\vec{R}_i} E(\vec{R}_i)\, n_i + \frac{1}{2}\sum_{\vec{R}_i}\sum_{\vec{R}_j} V_2(\vec{R}_i,\vec{R}_j)\, n_i n_j + \frac{1}{6}\sum_{\vec{R}_i}\sum_{\vec{R}_j}\sum_{\vec{R}_k} V_3(\vec{R}_i,\vec{R}_j,\vec{R}_k)\, n_i n_j n_k + \ldots , \quad (198)$$

$\{\vec{R}\}$ set of occupied cells, $n_i = 0$ or 1. Microscopic motion about equilibrium position neglected.

$P(\{\vec{R}\},t)$: probability that the system is in the state $\{\vec{R}\} = (n_1, n_2, \ldots, n_{N_c})$ at time t.

Time evolution $\rightarrow$ Master equation:

$$\frac{dP(\{\vec{R}\},t)}{dt} = \sum_{\{\vec{R}'\}} \Big[W(\{\vec{R}\},\{\vec{R}'\})\, P(\{\vec{R}'\},t) - W(\{\vec{R}'\},\{\vec{R}\})\, P(\{\vec{R}\},t) \Big] . \quad (199)$$

Self-diffusion on surfaces

Transition state theory $\rightarrow$ jump rate for a particle on a surface

$$k_{\rm j} = k_0 \exp\left(-\frac{E_a}{k_B T_s}\right) , \quad (200)$$

$P(\vec{R},t)$:Probability that surface site $\vec{R}$ on the surface is occupied a time t.

$P(\vec{R},t)$ satisfies diffusion equation

$$\frac{\partial P(\vec{R},t)}{\partial t} = D_s\, \nabla^2 P(\vec{R},t) . \quad (201)$$

with the *self-diffusion coefficient* D_s

$$D_s = \frac{k_{\rm j} a^2}{4} \quad (202)$$

Chemical diffusion coefficient

Ensemble of particles on the surface; conservation law:

$$\frac{\partial n(\vec{R},t)}{\partial t} + \nabla \cdot \vec{j}(\vec{R},t) = 0 \,, \tag{203}$$

Assumption: particle current driven by gradient of the density ⇒ *Fick's law*

$$\vec{j} = -D_c \, \nabla n(\vec{R},t) \,. \tag{204}$$

Fick's law + conservation law = Fick's second law:

$$\frac{\partial n(\vec{R},t)}{\partial t} = \nabla \cdot (D_c \nabla n(\vec{R},t)) \,. \tag{205}$$

D_c and D_s only for vanishing density equal

Hopping vs exchange diffusion

Hopping diffusion

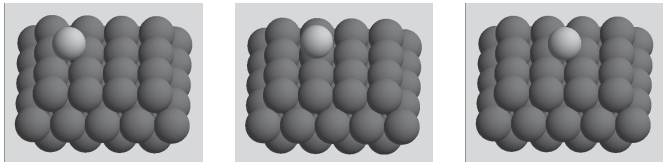

Exchange diffusion

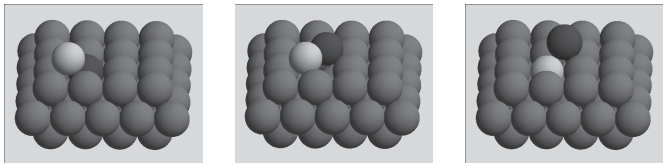

Exchange mechanism on Pt(001), Ir(001) and Al(001) favored because of threefold coordination at the transition state instead of twofold coordination

P.J. Feibelman, PRL **65**, 729 (1990)

Adsorption and desorption kinetics

Change of coverage: $$\frac{d\theta}{dt} = R_{ad} - R_{des} = \frac{S(\theta,T) P a_s}{\sqrt{2\pi m k_B T}} - R_{des} \tag{206}$$

Coverage in lattice gas model: $$\theta(t) = N_c^{-1} \sum_i \sum_{\{\vec{R}\}} n_i \; P(\{\vec{R}\},t) = N_c^{-1} \sum_i \langle n_i \rangle. \tag{207}$$

$$S(\theta,T) = S_0(T) \, \{(1-\theta) + \sum_{\{\vec{R}\}} \left(A_1 \sum_a \langle (1-n_i) n_{i+a} \rangle + A_2 \sum_{a,a'} \langle (1-n_i) n_{i+a} n_{i+a'} \rangle + \ldots \right) \Big\} \tag{208}$$

Detailed balance:

$$1 + A_1 = (1 + D_1) \exp(-V_{nn}/k_B T), \tag{209}$$

Assume: low T → no equilibrium during adsorption ⇒

$S(\theta,T)/S_0(T) = (1-\theta)^{z+1}$: $V_{nn} \gg k_B T$

$S(\theta,T)/S_0(T) = (1-\theta)\,(1+\theta)^z$: $-V_{nn} \gg k_B T$

z: number of nearest neighbors

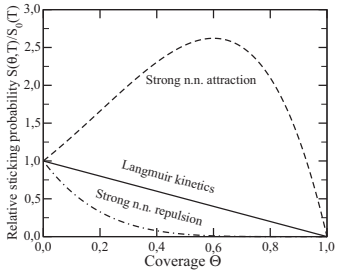

Temperature programmed desorption (TPD)

Simple n-th order desorption process: Relation T_{max}–E_{des}

$$\ln\left(\frac{T_{max} \; R_0 \; \theta^{n-1}}{\alpha}\right) = \frac{E_{des}}{k_B T_{max}} + \ln\left(\frac{E_{des}}{k_B T_{max}}\right) \,. \tag{210}$$

Often TPD spectra distorted due to lateral interactions, dynamical effects etc.
⇒ Realistic modelling necessary

Modelling of TPD

Desorption rate:

$$R_{des} = S(\theta,T) \, \frac{a_s}{\lambda_{th}^2} \, \frac{k_B T}{h} \, Z_{int} \, \exp(\beta\mu) \,. \tag{211}$$

O/Ru(0001) Lattice gas Hamiltonian:

1^{st}, 2^{nd} and 3^{rd} nearest-neighbor two-body interaction energies and nearest-neighbor three-body interactions determined by DFT calculations

Comparison theory-experiment

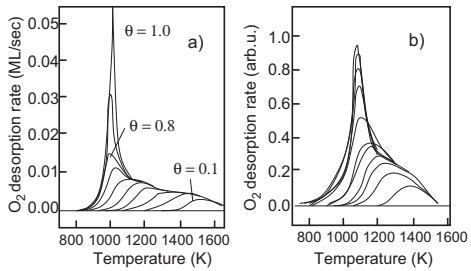

TPD spectra for the associative desorption of oxygen from Ru(0001). (**a**) theory, (**b**) experiment. (C. Stampfl *et al.* PRL **83**, 2993 (1999).)

Nonlinear phenomena on surfaces

Photoemission electron microscopy (PEEM) image of a Pt(110) surface exposed to $4{\times}10^{-4}$ mbar O_2 and $4.3{\times}10^{-5}$ mbar CO at a temperature of $T = 448$ K (A. Nettesheim *et al.*, JCP **98**, 9977 (1993)).

Theoretical modelling

Reaction scheme for the description of the CO oxidation on Pt(110)

$$\mathrm{CO} + * \leftrightarrow \mathrm{CO}^{(\mathrm{ads})}\,, \tag{212}$$
$$\mathrm{O_2} + * \rightarrow 2\mathrm{O}^{(\mathrm{ads})}\,, \tag{213}$$
$$\mathrm{O}^{(\mathrm{ads})} + \mathrm{CO}^{(\mathrm{ads})} \rightarrow 2* + \mathrm{CO_2} \tag{214}$$
$$1\times 2 \leftrightarrow 1\times 1\ . \tag{215}$$

Kinetics: $u = \theta_{\mathrm{CO}},\ v = \theta_{\mathrm{O}},\ w = \theta_{1\times 1}$

$$\dot{u} = s_{\mathrm{CO}}\, p_{\mathrm{CO}} - k_2 u - k_3 uv + D\nabla^2 u, \tag{216}$$
$$\dot{v} = s_{\mathrm{O_2}}\, p_{\mathrm{O_2}} - k_3 uv, \tag{217}$$
$$\dot{w} = k_5\,[f(u) - w], \tag{218}$$

Delayed inhibitor production

Growth modes on surfaces

Growth modes

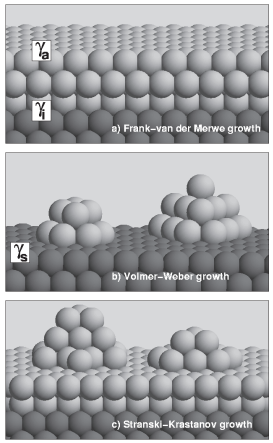

Illustration of three distinct growth modes.

Thermodynamics

Free surface energy of the substrate γ_s,
free surface energy of the adsorbate overlayer γ_a
substrate-adsorbate interface energy γ_i

$\gamma_a + \gamma_i < \gamma_s \Rightarrow$ 2D FV growth

$\gamma_a + \gamma_i > \gamma_s \Rightarrow$ 3D VW growth

Intermediate SK case: energy difference
$\Delta\gamma = \gamma_a + \gamma_i - \gamma_s$ changes sign at a critical layer thickness leading to a transition from 2D to 3D growth.

Kinetics

However, growth corresponds to a non-equilbrium situation, hence the resulting surface structures are governed by kinetics, not thermodynamics

Atomistic processes during growth

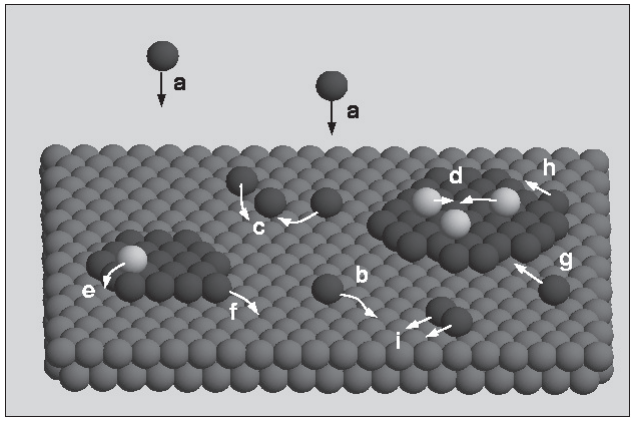

a) deposition, b) diffusion on terraces, c) nucleation of an island,
d) nucleation of a second-layer island, e) diffusion to a lower terrace,
f) attachment to an island, g) diffusion along a step edge, h) detachment from an island, i) diffusion of a dimer (or a larger island).

Nucleation theory

J.A. Venables, PRB **36**, 4153 (1987)

Assumption: clusters of size $j > i$ stable; i critical cluster size,
only single atoms mobile, n_x density of stable clusters:

$$n_x = \sum_{j=i+1}^{\infty} n_j \tag{219}$$

Rate equations for densities n_j of clusters of size j

$$\frac{dn_1}{dt} = F - \sigma_i D n_i n_1 - \sigma_x D n_x n_1 - F\theta \tag{220}$$

F deposition flux, $\sigma_i D n_1 n_i$ nucleation term, $\sigma_x D n_x$ diffusion capture rate,
θ coverage of stable clusters

$$\frac{dn_j}{dt} = 0\,, \qquad 2 \le j \le i\,. \tag{221}$$

Island density and critical cluster size

$$\frac{dn_1}{dt} = F - k_n n_1 - \sigma_x D n_x n_1 - F\theta \tag{222}$$

$$\frac{dn_j}{dt} = 0\,, \qquad 2 \le j \le i\,. \tag{223}$$

$$\frac{dn_x}{dt} = \sigma_i D n_1 n_i - 2n_x \frac{d\theta}{dt} \tag{224}$$

$\sigma_i D n_1 n_i$ nucleation term, $2n_x \frac{d\theta}{dt}$ disappearance of stable clusters due to coalescence

$\Rightarrow \ldots \Rightarrow$ steady-state scaling relation for density of stable islands:

$$n_x = f(\theta, i) \left(\frac{D}{F}\right)^{-\frac{i}{i+2}} \exp\left(\frac{E_i}{(i+2)k_B T}\right)\,. \tag{225}$$

E_i binding energy of a i-sized cluster

Scaling theory

Scaling relation for density of stable islands;

$$n_x \propto \left(\frac{D}{F}\right)^{-\frac{i}{i+2}}\,. \tag{226}$$

Scaling relation can be used to extract microscopic parameters from experiment

Island density n_x as a function of flux $F \Rightarrow$ critical size i

Temperature dependence of n_x for a known critical size i
$\Rightarrow$ diffusion barrier E_a and prefactor D_0

Simple scaling theory often works rather well, but it is only valid for compact islands in the coverage regime of saturation

Furthermore, as a mean-field theory it cannot properly describe island size distributions and coalescence effects

Microscopic approach needed

Closed-packed steps on fcc(111) surfaces

Two type of close-packed steps on fcc(111) surfaces:

{100} and {111} facets

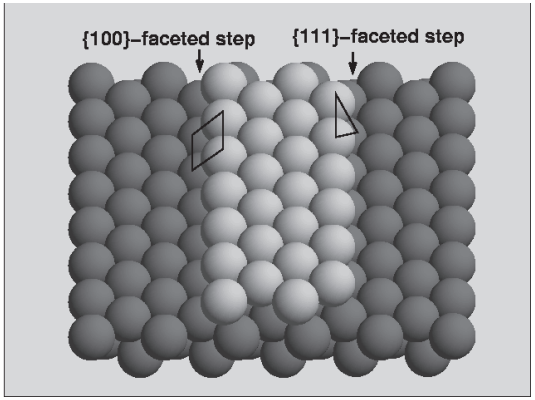

Step formation energies on Al(111): $E_{\{100\}} = 0.248$, $E_{\{111\}} = 0.232$ (eV/atom)

Diffusion mechanisms of Al/Al(111)

adatom diffusion	mechanism	E_a (eV)
flat Al(111)	hopping	0.04
parallel to {111}-faceted step	exchange	0.42
parallel to {100}-faceted step	hopping	0.32
descent down {111}-faceted step	exchange	0.06
descent down {100}-faceted step	exchange	0.08
corner jump (bridge)	hopping	0.17
corner jump (atop)	hopping	0.28

R. Stumpf and M. Scheffler, PRB **53**, 4958 (1996)

adatom diffusion	mechanism	Prefactor (cm^2/s)
flat Al(111)	hopping	2×10^{-4}
parallel to {111}-faceted step	exchange	5×10^{-2}
parallel to {100}-faceted step	hopping	5×10^{-4}

KMC simulation of the growth of Al(111)

Simulation (1/8 of simulation area = 600×600 array)

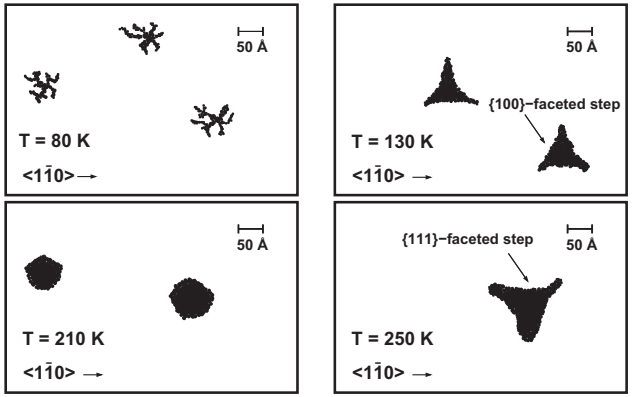

Deposition flux 0.08 ML/s, coverage $\theta = 0.08$ ML

P. Ruggerone *et al.*, Prog. Surf. Sci. **54**, 331 (1997)

Temperature dependence of the growth of Al(111)

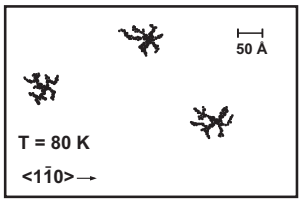

Low temperatures ($T = 50$ K): hit-and-stick

Diffusion limited aggregation ⇒ irreversible sticking to the site of first attachment

⇒ fractal (dendritic) growth

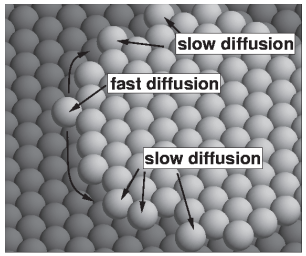

Higher temperatures ($T = 130 - 250$ K):

form of the islands determined by mobility along the steps

The lower the speed of migration along a given step edge, the higher the speed of advancement of this step edge

⇒ the step shortens and eventually disappears

Temperature dependence of the growth of Al(111)

Diffusion coefficient: $D = D_0 \exp(-E_a/k_B T)$

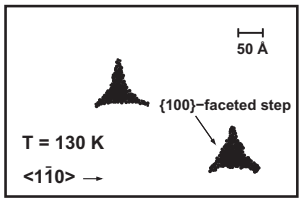

$T = 130$ K: triangular islands bounded by {100} steps

Diffusion barrier dominates diffusion coefficient

$E_a^{\{100\}} < E_a^{\{111\}}$

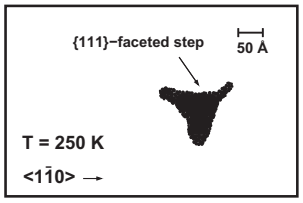

$T = 250$ K: triangular islands bounded by {100} steps

Prefactor dominates diffusion coefficient

$D_0^{\{100\}} < D_0^{\{111\}}$

$T = 210$ K: intermediate case

High temperatures $T \geq 400\ K$ ($E_{\{100\}} = 0.248$, $E_{\{111\}} = 0.232$ (eV/atom)):
Step formation energies determine equilibrium shape of the islands: $L_{\{100\}} : L_{\{111\}} = 4 : 5$

Growth of a compound semiconductor: GaAs

P. Kratzer and M. Scheffler, Phys. Rev. Lett. **88**, 036102 (2002).

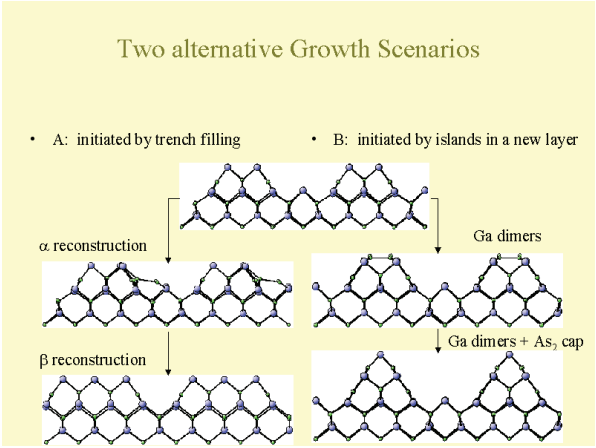

Growth determined by kinetics → KMC simulations

KMC simulations of GaAs growth

31 processes (barriers) explicitly considered by DFT, prefactor: $10^{13}\mathrm{s}^{-1}$

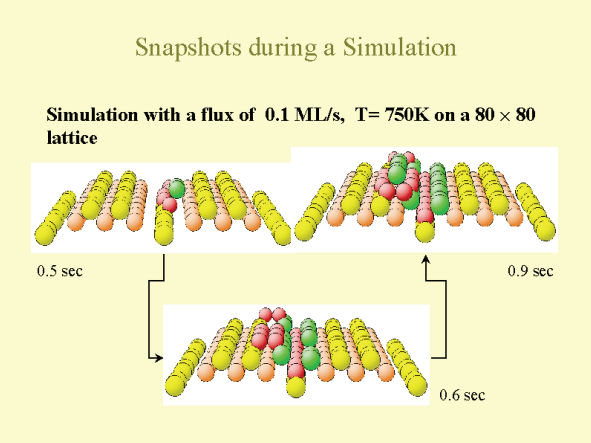

Bilayer structure → larger two-dimensional islands, which may coalesce
→ layer-by-layer growth.

Growth of a compound semiconductor: GaAs

31 processes (barriers) explicitly considered by DFT as an input for KMC simulations, prefactor: $10^{13}\mathrm{s}^{-1}$

P. Kratzer and M. Scheffler, Phys. Rev. Lett. **88**, 036102 (2002).

Front view

Top view

Island density on GaAs(100)

Island density

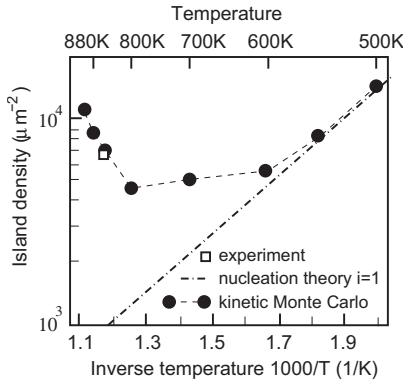

Calculated island density of GaAs(100) (P. Kratzer and M. Scheffler, PRL **88**, 036102 (2002)).

Discussion

Island density determined for temperatures between 500 K and 900 K.

$T \leq 600$ K: Nucleation theory and kinetic Monte Carlo simulations agree

$T > 600$ K: Deviation between nucleation theory and kinetic Monte Carlo simulations

$T > 800$ K: Island density rises with increasing temperature which can not be understood at all within nucleation theory

Reason: At elevated temperatures, Ga-As-As-Ga_2 complexes that form the island nuclei are no longer stable. However, due to higher mobility of Ga adatoms nucleation rate increases.

Electronically nonadiabatic processes at surfaces

Problems associated with incorporating electronic transitions

Determination of the electronically excited states:

DFT yields total energies explicitly only for the electronic ground state

⇒ Quantum chemistry methods or time-dependent DFT

Calculation of coupling matrix elements between these excited states

For processes with electronic transitions, matrix elements between different electronically excited states are needed, but electronic structure methods usually only give the eigenenergy spectrum

Simulation of the reaction dynamics with electronic transitions

Dynamics of electrons have to be treated quantum mechanically which can become quite cumbersome if many electrons are involved

Time-dependent density functional theory (TDDFT)

E. Runge and E.K.U. Gross, Phys. Rev. Lett. **52**, 997 (1984).

Runge-Gross theorem:

The densities $n(\vec{r},t)$ and $n'(\vec{r},t)$ evolving from a common initial state $\Psi_0 = \Psi(t_0)$ under the influence of two potentials $v(\vec{r},t)$ and $v'(\vec{r},t)$ are always different provided that the potentials differ by more than a purely time-dependent, i.e. $\vec{r}$-independent function $v(\vec{r},t) \neq v'(\vec{r},t) + c(t)$

$\Rightarrow$ One-to-one mapping between time-dependent potentials and time-dependent densities (Note that the functional depends on $\Psi_0 = \Psi(t_0)$)

Proof

a little bit more involved than for time-independent DFT:
First show by using the quantum mechanical equation of motion that the current densities
$\vec{j}(\vec{r},t) = \langle \Psi(t)|\hat{\vec{j}}_p|\Psi(t)\rangle$ and $\vec{j}'(\vec{r},t) = \langle \Psi'(t)|\hat{\vec{j}}_p|\Psi'(t)\rangle$
are different for different potentials v and v' and then use the continuity equation
$\frac{\partial}{\partial t}(n(\vec{r},t) - n'(\vec{r},t)) \;=\; -\nabla\cdot(\vec{j}(\vec{r},t) - \vec{j}'(\vec{r},t))$

Excitation energies calculated using TDDFT

M. Petersilka, U.J Gossmann and E.K.U. Gross, Phys. Rev. Lett. **76**, 1212 (1996).

Kohn-Sham response function of non-interacting particles with unperturbed density n_0:

$$\chi_s(\vec{r},t,\vec{r}',t') \;=\; \left.\frac{\delta n[v_s](\vec{r},t)}{\delta v_s(\vec{r}',t')}\right|_{v_s[n_0]} . \tag{227}$$

Define the *time-dependent exchange-correlation kernel*

$$f_{\rm xc}[n_0](\vec{r},t,\vec{r}',t') \;=\; \left.\frac{\delta v_{\rm xc}[n](\vec{r},t)}{\delta n(\vec{r}',t')}\right|_{n_0} . \tag{228}$$

True excitation energies $\Omega_j = E_j - E_0$: frequencies where the eigenvalues $\lambda(\omega)$ of

$$\int d^3\vec{x} \int d^3\vec{r}'\, \chi_s(\vec{r},\vec{r}',\omega)\left(\frac{1}{|\vec{r}'-\vec{x}|} + f_{\rm xc}[n_0](\vec{r}',\vec{x},\omega)\right) g(\vec{r}',\omega) \;=\; \lambda(\omega)\, g(\vec{r},\omega) \tag{229}$$

satisfy

$$\lambda(\Omega) = 1 \tag{230}$$

Lifetimes of electronic excitations at metal surfaces

Damping rate Γ, i.e. inverse lifetime of an electron with $\epsilon_i > E_F$:

$$\Gamma = \tau^{-1} = -2\int d^3r \int d^3r' \phi_i^*(\mathbf{r}) \Im\Sigma(\mathbf{r},\mathbf{r}',\epsilon_i)\phi_i(\mathbf{r}') \tag{231}$$

$\Sigma(\mathbf{r},\mathbf{r}',\epsilon_i)$: Non-local self-energy operator, determined in the GW approximation in terms of the screened interaction:

$$\Im\Sigma(\mathbf{r},\mathbf{r}',\epsilon_i > E_F) = \sum_f{}' \phi_f^*(\mathbf{r}')\Im W(\mathbf{r},\mathbf{r}',\omega)\;\phi_f(\mathbf{r}) \;, \quad \omega = \epsilon_i - \epsilon_f \tag{232}$$

Homogeneous electron gas in the high-density limit:

$$\tau = \frac{263}{r_s^{5/2}(E-E_F)^2}(\text{fs}) \tag{233}$$

Finite lifetime of excited states due to electron-electron, electron-phonon and electron-defect scattering

Surface and image potential states at Cu surfaces

Projected bulk band structure

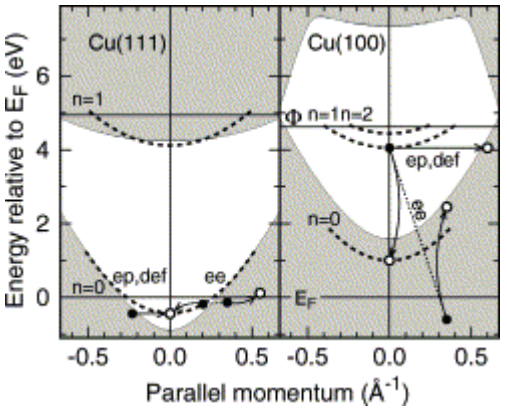

P. Echenique *et al.*, Surf. Sci. Rep. **52**, 219 (2004)

Electronic states

$n = 0$: surface states

$n \geq 1$: image potential states

Scattering mechanisms:

Electron-electron (ee) scattering inelastic

Electron-phonon (ep) and electron defect (def) scattering elastic

Photohole self-energy on Mo(110)

Self-energy

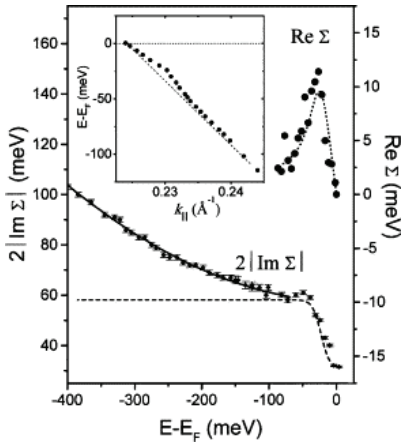

Photohole self-energy for a d-like surface state on Mo(110)
(P. Echenique *et al.*, Surf. Sci. Rep. **52**, 219 (2004))

Discussion

Rapid increase up to $E_i \approx$ -40 meV and then a slower increase further away from E_F

Solid line for energies below -80 meV: quadratic fit
$\Rightarrow$ electron-electron scattering

Dotted (dashed) line: Calculated Re (Im) Σ for electron-phonon scattering

ep contribution to Im Σ has to be shifted upwards by 26 meV:
$\Rightarrow$ electron-defect scattering

Electronically excited potentials at surfaces

Potential energy surfaces

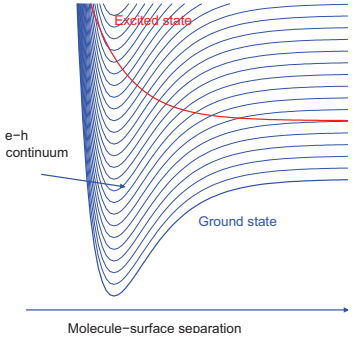

Excitation mechanisms

Molecular states couple to the electron-hole (e-h) pair continuum of the metal surface
Excitation of e-h pairs hardly changes molecule-surface-potential

$\Rightarrow$ Influence of the excitation of e-h pairs on molecule surface dynamics can be described within a friction-dissipation formalism

Electronic excitation of the molecule or atom interacting with the surface
Shape of potential might be entirely different from ground-state potential

Potential of excited state must be explicitly considered

Molecular dynamics with electronic friction

M. Head-Gordon and J.C. Tully, J. Chem. Phys **103**, 10137 (1995)

Molecular dynamics

Equation of motion for adsorbate

$$M_I \ddot{\vec{R}}_I = -\frac{\partial V}{\partial \vec{R}_I} - \sum_j K_{IJ} \dot{\vec{R}}_J + \vec{S}_I(t) \quad (234)$$

$\vec{S}_I(t)$ stochastic fluctuating force satisfying the fluctuation-dissipation theorem

$$\left\langle \vec{S}_I(t) \vec{S}_J(t') \right\rangle = k_B T K_{IJ} \delta(t - t') \quad (235)$$

K_{IJ} friction matrix in the adsorbate degrees of freedom, dependent on the position

Friction matrix

Assumption: weak coupling and smooth metal density of states at the Fermi level

$$K_{IJ} = \pi\hbar \, \mathrm{Tr}\{P(\varepsilon_F) \vec{G}_{\vec{R}_I} P(\varepsilon_F) \vec{G}_{\vec{R}_J}\} \quad (236)$$

with

$$\vec{G}_{\vec{R}_I} = \frac{\partial}{\partial \vec{R}_I} H - \varepsilon_F \frac{\partial}{\partial \vec{R}_I} S \quad (237)$$

and split-time local density of states

$$P(\varepsilon, t, t') = \sum_i c_i(t) c_i(t') \delta(\varepsilon - \varepsilon_i) \quad (238)$$

Energy independent K_{IJ} has been evaluated for CO/Cu(111) by Hartree-Fock cluster calculations using single excitations

Role of e-h pairs in the scattering and sticking of CO/Cu(111)

J.T. Kindt *et al.*, J. Chem. Phys **109**, 3629 (1998)

Sticking

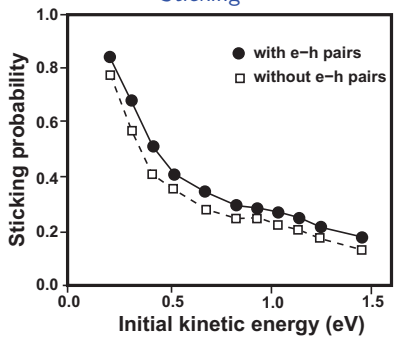

Scattering

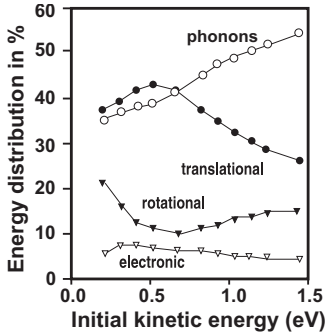

e-h pair excitation only plays a minor role as a dissipation channel in the sticking and scattering of CO/Cu(111)

Description of light or electron stimulated desorption

DIET: Desorption Induced by Electronic Transitions

Menzel-Gomer-Redhead scenario

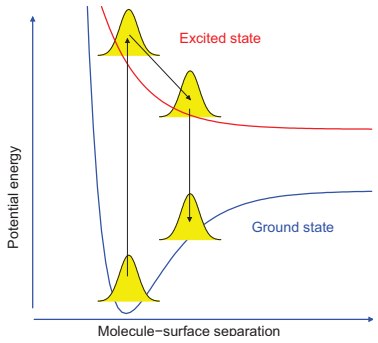

Wave packet dynamics

- Light- or electron stimulation leads to transition of the wave packet onto the excited potential energy surface
- Wave packet propagates in excited state with a certain lifetime τ and then returns to the ground state in a Franck-Condon transition
- If the gain in the kinetic energy on the excited state is larger than the remaining desorption barrier, the wave packet will desorb

Laser-induced desorption of NO/NiO(100)

Charge transfer PES

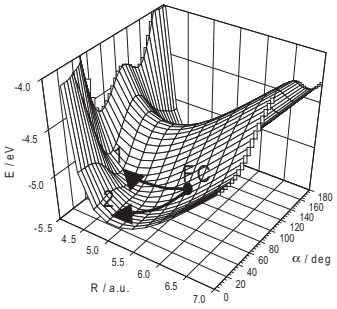

PES calculated in a embedded-cluster model in a truncated CISD scheme (dd-excitations omitted)

(T. Klüner *et al.*, PRL **80**, 5208 (1998)).

Measured and calculated velocity distributions

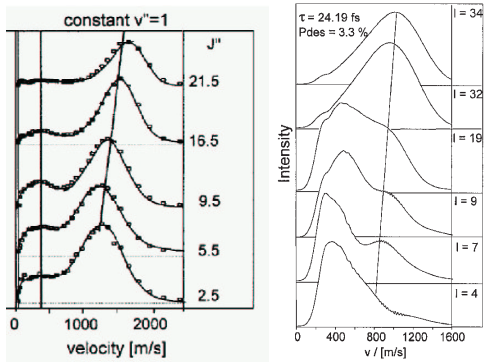

(Exp: T. Mull *et al.*, JCP **96**, 7108 (1992), Theory: T. Klüner *et al.*, PRL **80**, 5208 (1998)).

Measured bimodal velocity distribution qualitatively reproduced in wave-packet calculations

Mixed quantum-classical description of DIET

Potential energy surfaces

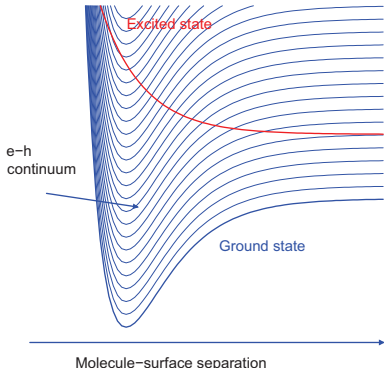

Mixed quantum-classical description

Wave function:

$$\Psi(\mathbf{r},\mathbf{R},t) = c_1(t)\Phi_{e^-}(\mathbf{r},\mathbf{R}) + \Phi_c(\mathbf{r},\mathbf{R},t) \quad (239)$$

Influence of Φ_c expressed trough an optical potential (W. Brenig, Z. Phys. B 23, 361 (1976)) $\Rightarrow$ Schrödinger equation:

$$i\hbar\dot{c}_1 \;=\; V_{e^-}(\mathbf{R})c_1(t) \;+\; i\Delta(\mathbf{R})c_1(t) \quad (240)$$

Δ width of the resonance

$$\Delta(E) \;=\; \pi \sum_{\mathbf{k}} |V_{e^-\mathbf{k}}|^2 \delta(E-\varepsilon_{\mathbf{k}}) \quad (241)$$

Δ often parametrized as

$$\Delta(z) \;=\; \Delta_0\, e^{-2\gamma z} \quad (242)$$

Modelling of DIET processes

Potential energy surfaces

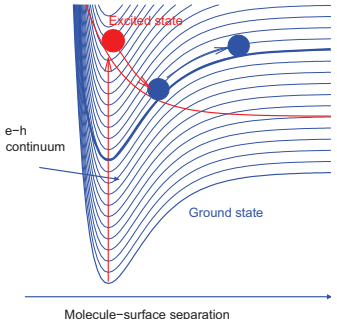

Algorithm

(cp. P. Saalfrank, Chem. Phys. **211**, 265 (1996).)

- Start with mixed-classical simulation after the first Franck-Condon transition on the excited state surfaces
- The norm of the wave function decreases due to the presence of the optical potential $\Delta(E, Z, \ldots)$
- Comparison with random number $\Rightarrow$ Franck-Condon transition to the molecular ground state with the excess energy taken up by the substrate
- $\rightarrow$ Adiabatic ground state molecular dynamics in order to determine desorption distributions

Ab initio 2D PES empirically extended to seven dimensions including one surface oscillator

C. Bach, T. Klüner, and A. Groß, Chem. Phys. Lett. **376**, 424 (2003); Appl. Phys. A **78**, 231 (2004).

NO/NiO(100): Desorption rate and desorption channels

C. Bach, T. Klüner, and A. Groß, Chem. Phys. Lett. **376**, 424 (2003); Appl. Phys. A **78**, 231 (2004).

Desorption rate

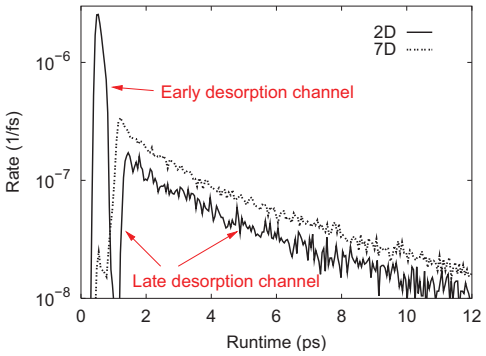

Early and late desorption channel present in the photon-induced desorption

Desorption channels

Early desorption channel: directly scattered molecules with high kinetic energies

Late desorption channel: dynamically trapped molecules with lower kinetic energies

Desorption rate drops practically to zero after 1.2 ps: Computationally demanding wave-packet calculations stopped after this time ⇒ late desorption channel overlooked

Early vs late desorption channels in 2D

Velocity distributions

Early desorption channel

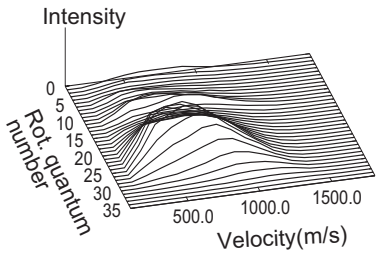

Late desorption channel

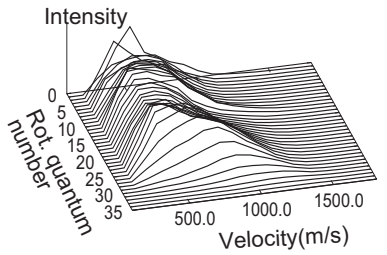

Early desorption channel: directly scattered molecules with high kinetic energies

Late desorption channel: dynamically trapped molecules with lower kinetic energies

Desorption probabilities and rotational temperatures

Desorption properties

	2D	3D	6D	7D
P_{des} (%)	4.84	3.63	4.74	4.02
P_{early} (%)	2.93	0.32	2.53	0.32
E_{rot} (K)	770	366	883	395

Incorporation of surface oscillator:

⇒ suppression of the early desorption channel and of high rotational excitations

⇒ total desorption yield only slightly modified

Rotational temperatures of the 3D and 7D calculations in better agreement with experimental results ($T_{\mathrm{rot}}^{\mathrm{exp}} = 260 - 470$ K)

Rotational distribution

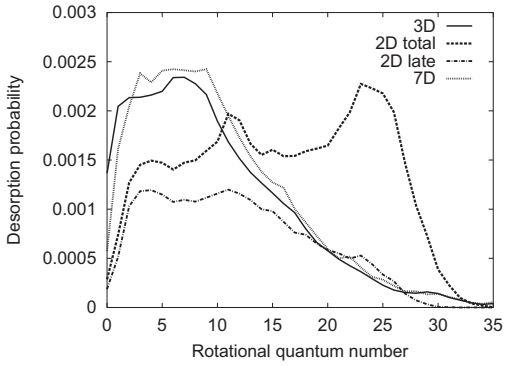

Significant influence of dissipation on the desorption properties

Velocity distribution in the laser induced desorption of NO/NiO(100)

Early desorption channel in 2D

Quantum

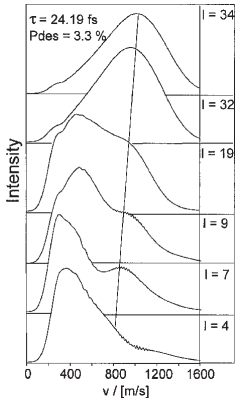

Mixed quantum-classical

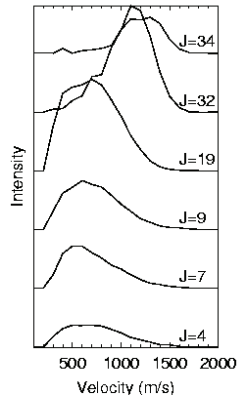

7D calculations

Mixed quantum-classical

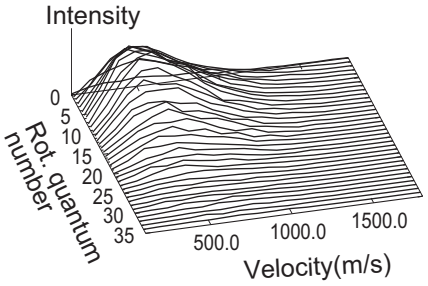

Good agreement between 2D quantum and mixed quantum-classical calculations

No bimodality in the velocity distribution of the 7D calculations

Bimodality in the velocity distributions

Bimodality not reproduced in high-dimensional mixed-quantum classical simulations

Total velocity distribution

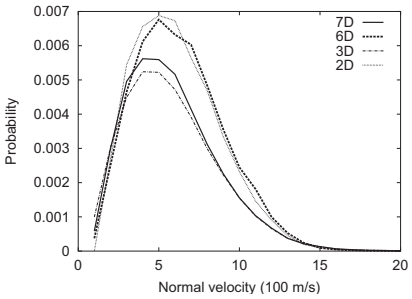

Discrepancy between theory and experiment

Possible reasons

- Empirical extension of the *ab initio* PES to seven dimensions incorrect
- More than one excited state involved in the laser-induced desorption dynamics
- More complex, spatially varying transition probability needed

Outlook: Challenges I

Indium cluster on Si(111)(7×7)

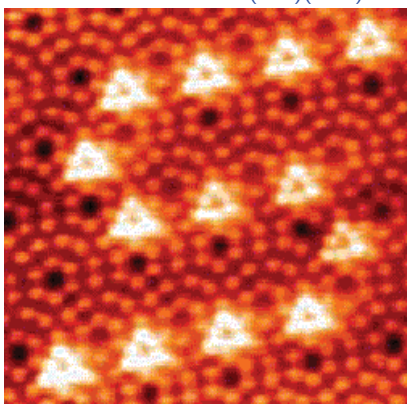

J.-L. Li *et al.*, Phys. Rev. Lett. **88**, 066101 (2002)

Nanoscience

- Nanoscience and nanotechnology rapidly growing research field
- *Ab initio* treatment of nanostructures computationally demanding, but still feasible
- Nanostructures also interesting from a fundamental point of view: quantum size effects, self-ordering phenomena, chemical reactivity, etc.
- Example: Spontaneous assembly of In clusters on Si(111)(7×7)
  J.-L. Li *et al.*, Phys. Rev. Lett. **88**, 066101 (2002)
  CO oxidation on Au_8 clusters adsorbed on MgO
  A. Sanchez *et al.*, J. Phys. Chem. A **103**, 9573 (1999)

Outlook: Challenges II

Supercell approach

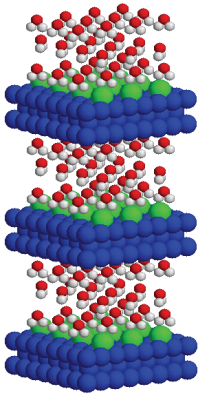

Slab model with the space between the layer filled with water

Reactions at the liquid-solid interface

- Space between the slabs can also be filled with a liquid instead of leaving it empty
- Such an approach allows the study of phenomena at the solid-liquid interface
- ⇒ Problems related to electrochemistry can be addressed such as, e.g., reactions relevant for fuel cells
- Example: Deprotonation of acetic acid over Pd(111)
  Water stabilizes the ionic products formed on the metal surface
  S.K. Desai *et al.*, J. Phys. Chem. B **105**, 9171 (2201).

Outlook: Challenges III

Cu^{2+} binding at a prion protein

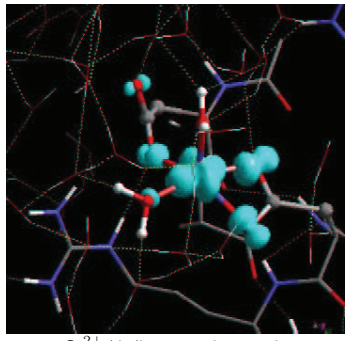

Cu^{2+} binding at a prion protein
(J. VandeVondele and U. Röthlisberger)

Biochemical problems

- Understanding of enzymatic processes at the molecular level is a challenging problem in (bio)chemistry
- Protein > 1000 atoms, solvent > 10000 atoms
  Active site ∼ 100 atoms
- ⇒ Combined ab initio molecular dynamics/molecular mechanics approach required
- Example: Binding sites of Cu^{2+} at a prion protein
  J. VandeVondele and U. Röthlisberger, ETH Zürich